

Realisation of an experimental flexible beam set-up

Citation for published version (APA):

van Eeghem, J. S. (1993). *Realisation of an experimental flexible beam set-up*. (DCT rapporten; Vol. 1993.180). Technische Universiteit Eindhoven.

Document status and date:

Published: 01/01/1993

Document Version:

Publisher's PDF, also known as Version of Record (includes final page, issue and volume numbers)

Please check the document version of this publication:

- A submitted manuscript is the version of the article upon submission and before peer-review. There can be important differences between the submitted version and the official published version of record. People interested in the research are advised to contact the author for the final version of the publication, or visit the DOI to the publisher's website.
- The final author version and the galley proof are versions of the publication after peer review.
- The final published version features the final layout of the paper including the volume, issue and page numbers.

[Link to publication](#)

General rights

Copyright and moral rights for the publications made accessible in the public portal are retained by the authors and/or other copyright owners and it is a condition of accessing publications that users recognise and abide by the legal requirements associated with these rights.

- Users may download and print one copy of any publication from the public portal for the purpose of private study or research.
- You may not further distribute the material or use it for any profit-making activity or commercial gain
- You may freely distribute the URL identifying the publication in the public portal.

If the publication is distributed under the terms of Article 25fa of the Dutch Copyright Act, indicated by the "Taverne" license above, please follow below link for the End User Agreement:

www.tue.nl/taverne

Take down policy

If you believe that this document breaches copyright please contact us at:

openaccess@tue.nl

providing details and we will investigate your claim.

Realisation of an experimental flexible beam set-up

Jean van Eeghem

TPD-HAG-RPT-94-0109

WFW Rapport 93.180

STAGEVERSLAG

Realisation of an experimental flexible beam set-up

Jean van Eeghem

TNO-TPD-HAG

coach (TNO-TPD): Teun van den Dool

coach (TU Eindhoven): Frans Veldpaus

Delft, February 1994

Abstract

Currently, most industrial manipulators use controllers that do not take the flexibility of links into account. To position the final link that holds a tool or a payload (end-effector), often classical PD-controllers are used. In most cases these controllers give an acceptable performance because of the extreme rigidity of the links.

In order to develop a new generation of industrial manipulators that can operate at higher speeds or with lower power consumption, the mass of the rigid links must be reduced. The reduction of the link mass leads to a more flexible construction in which it is no longer acceptable to neglect the deformation of the link due to bending forces. Such a link will be referred to as a "flexible beam". To maintain accuracy in positioning the end-effector, the displacement due to the flexibility must be taken into account by the controller.

The model of a flexible beam presented by I. Kruijs (Chapter 3) shows that we are dealing with a non-minimum phase system. Simulations with this model using a feedback controller show that the first mode of the flexible beam is the most significant one. It is possible to position the beams tip (with limited accuracy) by controlling this mode.

In literature many flexible beam controllers are presented. Computed torque controllers show the best performance, but this is hardly verified by experiments.

This report deals with the realisation of an experimental flexible beam set-up to test different controllers presented in literature. Up to now a feedback controller is implemented on the set-up. This controller rapidly damps out the occurring oscillations but is restricted by input saturation of the servo-amplifier.

Subjects that require further investigation are the influence of the non linearity of the servo-amplifier, the effect of the sensor mass on the flexible beam, the modelling of the friction occurring in the system and the implementation of more advanced controllers.

Contents

Abstract	3
Introduction	5
Literature Review	7
2.1 Introduction	7
2.2 Static compensation control.....	7
2.3 Output Feedback controllers.....	8
2.4 Computed torque controllers	9
Model of a flexible beam.....	11
3.1 Introduction.....	11
3.2 Model of a flexible beam with payload	11
3.3 Actuator model.....	14
Experimental set-up	16
4.1 Introduction.....	16
4.2 Dimensioning of the flexible beam.....	16
4.3 Sensors	20
4.4 Servomotor	23
4.5 Composition of the set-up.....	24
Controller design for a flexible beam	25
5.1 Introduction.....	25
5.2 P-controller	25
5.3 Output-Feedback controller	26
5.4 Simulations.....	27
5.5 Experiments	29
Conclusions.....	30
Recommendations	30
Bibliography.....	32
Appendix A	34
A.1 Flexible beam model	34
A.2 Derivation of $\varphi(X)$	39
Appendix B.....	43
B.1 Differential equation transformation	43
B.2 Calculation of α_n	45
Appendix C.....	46
Appendix D	48
Appendix E	51
SIMBEAM.M	51
STATE.M.....	53
GAMMI.M.....	54
CI.M	55
SIMULAT.M	55
Appendix F	57

Chapter 1

Introduction

In a recent survey (Journal A, ABB survey on Robotisation today, München, 1992) on world-wide robotisation, Japan is being pointed out as world leader in the deployment of robots. Japan has 16 robots stationed for each 1000 production workers. With an average of 2 or 3 robots per 1000 workers, the rest of the industrialised world forms an enormous potential market. Furthermore, market analyses reveal a continued growth even for Japan itself. As a result optimists among the producers of industrial automation systems believe that their mean annual turnover will keep growing by 10% for the next number of years. In absolute figures, 300.000 robots are being deployed world-wide (of which 180.000 in Japan).

The estimations of the future market for industrial manipulators justify further research on the improvement of these products. The survey also mentioned the expectations regarding the future of robotisation; besides more quality and reliability of the production process, approximately 60% of the automated industry expected production costs to decrease and production speed to increase. In this respect, improvement can be achieved by increasing the working speed, and by decreasing power consumption of the actuators. Either of these goals can be reached by lowering the weight of manipulator links. Because of the heavy weight link constructions, in present manipulator configurations the payload to robot mass ratio varies between 3 to 5%.

Robots (in general: industrial manipulators) can be used for trajectory tasks (welding, assembly or glueing) and pick and place tasks (materials handling or spot welding). In this report only position control will be considered. The rigid heavy weight links allow the deformation due to the bending forces to be neglected. Therefore controllers that position the end-effector (this is the point on the final link with the payload) only need to control as many degrees of freedom as there are links. With a position sensor attached to every link, the end-effector can be positioned for instance with a PD-controller. In general, when the link's weight is reduced it becomes more flexible. In case of a flexible link, negligence of bending forces is no longer acceptable and the effect of flexibility has to be compensated by the controller. The aim of this report is to give an introduction to the modelling and control of a flexible beam. It must be emphasised that the controllers presented in this report are no solution to the general problem of flexible manipulators.

At TNO Institute of Applied Physics (TPD) a project is initiated to obtain an experimental set-up to be able to test flexible beam controller performance. Although many articles have been published about different concepts of flexible beam control, very few articles deal with the practical verification of these theories. The experimental set-up enables us to implement and compare the controllers presented in literature. In Chapter 2 a literature review on this subject is presented. The review is divided in static deflection-, feedback- and computed torque controllers.

In Chapter 3 a model for the flexible beam is presented. It shows that a flexible beam has an infinite number of DOF's (degree of freedom) or modes. Theoretically speaking an infinite number of sensors is necessary to control the beam with a feedback controller. However in our case only a few of the doffs are significant for the displacement of the end effector. This allows the feedback of these significant modes in order to control the end effector.

Chapter 4 describes the experimental set-up that is recently installed at TPD. The experimental set-up of a flexible beam will be used to verify the results of the simulations described in Chapter 5. The actuator of the system is a servomotor/gearbox combination with amplifier. On the shaft of the gearbox a hub is installed which clamps the flexible beam.

A design for a feedback controller is given in Chapter 5. In this controller only one vibration mode (the most significant mode) is fed back. The performance of this controller is compared with a conventional PD-controller as used for rigid links.

Chapter 6 presents conclusions and recommendations for future research.

Chapter 2

Literature Review

2.1 Introduction

To be able to control light weight links, a thorough knowledge of the consequences of flexibility is necessary. By reducing the weight of the links, the displacements due to bending forces can no longer be neglected. The links change from rigid to flexible beams and the payload to robot mass ratio can now be increased to a 100 % or more. An existing example of a light weight link is the cable of a building-crane, with link to payload mass ratios of far over 100%. The deformations due to bending forces in the link, make accurate position control of the end effector more difficult than in the rigid case.

An often used solution to the problem of flexibility is to only compensate for the static deflection. Literature concerning this kind solution is regarded in the next section.

The dynamic flexible beam controllers can be divided into two groups. The first group consists of controllers based on feedback of the displacement (and eventually time-derivatives) of the end-effector. The second group calculates the input signal of the system by using the known system dynamics. These controllers are known as computed torque controllers, and are sometimes combined with a feedback controlloop.

In this Chapter a literature review is presented. The three kinds of controllers will be discussed separately in sections 2.2, 2.3 and 2.4.

2.2 Static compensation control

In "Modelleringsalgoritmen voor Industriële robots" written by F. Lucassen ('90) a solution to static deflection with FEM methods is presented. The control methods suggested are both model based, i.e. MRAC (Model Reference Adaptive Control) and Inverse dynamics (equals computed torque), but they do not account for the flexibility during the movements. Additionally an advanced measurement system for the position of the end-effector is used. This is a Laser interferometer that is capable to detect displacements less than 0.1 mm so that the amplitudes of the higher modes (above 100 Hz) can be detected (this is necessary in case of dynamic control of flexible links).

"Implementation of a flexible link model in a designed robot system using finite element method" by K. Drent ('88), discusses the deflection of the end effector due to flexibility of the link. The goal set by Drent is to improve positioning accuracy by compensating the static deflection (deflection due to gravity forces). After compensation a payload of 35 kg can be positioned with an accuracy of 0.05 mm, which is a remarkable result.

2.3 Output Feedback controllers

These controllers use the measurements of the systems sensors to create an input signal. Often these controllers use known system dynamics to observe states, or to calculate the feedback gain.

In "Perturbation techniques for flexible manipulators" A.R. Fraser ('91) describes different modelling techniques to simulate the system response. Some feedback controllers are tested at different positions in the closed loop. The goal of the controller is to provide extra damping of the transversal vibration modes. The best overall performance was given by the controller in the feedback path. This result supports the controller design of the experimental set-up. A second useful conclusion concerns the influence of the endmass on the system stability; a varying payload might result in an unstable closed loop response of a non varying controller.

In "Aktive schwingungsdämpfung an einem elastischen knickarmrobot" H. Henrichfreise ('87) uses state-feedback control. Because not all states can be measured a (model based) observer is added. This observer is non-linear and can observe the unknown states much better than its linear version. This improved performance is compared to conventional observers, and is found to be superior.

The Ph.D. thesis "Modelling and control of a flexible beam and robot arm" written by I. Kruijs ('90) discusses the complete process of modelling, controller design and experimental set-up. An abstract of the model is printed in Chapter 3 and Appendix A of this report. The controller design is based on feedback of the systems state. Two state-feedback controllers are presented, namely a LQG controller and a pole placement controller. Furthermore a robust controller design is presented. These controllers are compared to a conventional PD-controller that neglects the flexibility of the beam. Although the model of the flexible beam has an infinite number of modes, Kruijs assumes that for the beam deflection only the first 3 modes are significant. Next to a one-link experimental set-up, he also describes a two-link

robot arm including controller design. Both set-ups operate in a horizontal plane and show an acceptable performance compared to the PD-regulator.

"Active vibration control of a motor system by H_{∞} control" by Shigeto Ouchi et al. ('92) deals with a H_{∞} controller that reduces the torsional shaft vibrations by filtering (weighting) in- and output signals. Only one vibration mode is regarded and the higher modes are treated as plant uncertainty. This uncertainty can be translated into an output weighting function. Weighting functions together with known systems dynamics result in a feedback controller (fourth order) that suppresses higher vibration modes. The performance of this control approach is compared to a traditional PI-controller and is found to be superior in suppressing higher vibration modes. This result might also be useful in case other model uncertainties like friction occur.

2.4 Computed torque controllers

Computed torque controllers use the known system dynamics to calculate the system input. The desired setpoint or trajectory is used as an input for the inverse dynamics. The output of this calculation is equal to the input signal needed to make the system follow the desired movement. A problem with computed torque controllers, is that the flexible beam system has

more doffs than outputs. The flexible beam with payload has a regular system matrix but when calculating on-line we can encounter numerical problems. Mostly these problems result in an unstable solution for the desired movement.

"An inverse dynamics based closed-loop trajectory tracking control for a flexible arm" by E. Bayo ('91) presents a controller that combines the output of an inverse dynamics algorithm with a Linear Quadratic Gaussian regulator (LQG). Because the model used for inverse dynamics is never exact (due to friction or other unmodelled dynamics), the LQG controller is added for compensation of tracking errors. A major disadvantage is that the inverse dynamics process is executed off-line. A movement can only be performed after some calculation time and the off-line algorithm leaves no hope for possible adaptive features. Nevertheless the simulations show that in spite of the rapid movement, no vibrations are excited. Furthermore the control algorithm seems robust against disturbances at the hub and errors in the tip position.

"Tracking control of a non-minimum phase flexible manipulator" written by D. Kwon and W. Book ('91) presents the same kind of controller as the above mentioned paper. Again the computation of the system input is done off-line. Besides the input torque, the desired

trajectories of flexible co-ordinates are calculated. These flexible co-ordinates enable additional feedback control for optimal tracking performance. The controller designs are tested on an experimental set-up for zero- and non zero initial conditions. For the non zero conditions the flexible co-ordinates are divided into a rigid body component, a causal and an anticausal part. In this way the effect of the non zero initial condition will only influence the anticausal part. For the rigid body component and the causal part a known non zero condition will be canceled by taking it into account in the calculation of the system input. The controller presented in the article is said to have a fast tracking convergence in spite of small initial tracking errors. The author explicitly states that the non-minimum phase behaviour of the flexible beam can be cancelled by the inverse dynamics controller.

A recent Ph.D. thesis by I. Lammerts called "Adaptive Computed Reference Computed Torque Control of Flexible Manipulators" ('93) describes an on-line method to calculate an input signal with an extended version of computed torque control (CTC). In spite of the numerical problems in the case of on-line computation of unknown reference trajectories, the results are satisfying. If a numerical solution for the on-line computation problem can be found, adaptive CRCTC will enhance the performance of this controller. The control technique presented by Lammerts offers a general solution to the problem of flexibility, and it might be interesting to implement it on an experimental flexible beam set-up.

In a masters thesis written by D. Heijman various control techniques are presented. A fuzzy logic controller defined in an article by J.V. Kim (Vibration control of a flexible beam using Fuzzy Control Theory) is found to perform very badly. Furthermore a pole placement controller is described for setpoint control and its results were said to be good. For trajectory control, part of CRCTC theory is used, to generate bounded desired trajectories. Analytically determined trajectories result in good performance, however if this done by numerical integration the results are not satisfying. The model presented for a flexible beam also includes (high speed) non linear terms. Therefore it might be interesting to use this modelling in future research.

Chapter 3

Model of a flexible beam

3.1 Introduction

In order to simulate the behaviour of flexible beams we must derive a model. We also need this model to implement the model based controllers. In many articles models are given for flexible beams. In this report an abstract of the derivation in "Modelling and control of a flexible beam and robot arm" by I. Kruse is given. Because the model of a flexible beam carrying a payload is fairly general, this derivation is presented. In section 3.2 the model of the system actuator will be added to the flexible beam model.

3.2 Model of a flexible beam with payload

The derivation of the model can be found in Appendix A.1 The assumptions made for this derivation are:

- The material behaviour is isotropic linear elastic with Young's modulus E
- The beam axis is inextensible
- The deflections due to flexibility of the beam are small compared to the length of the beam ($W(X,t) \ll L$)
- In the stress-free situation the beam cross section is rectangular with cross sectional area A and length L
- There is no shear deformation
- The velocity of the imaginary rigid body movement is small compared to the lowest angular velocity of the occurring flexible modes ($\dot{\theta}_b \ll \omega_1$)
- Translations as a rigid body are suppressed by fixation of the hub (origin, see figure 3.1) to the ground.

The deflection of the beam is approximated by the function $W(X,t)$ that is a sum of products of a time depending part $q(t)$ and a position depending part $\varphi(X)$:

$$W(X,t) = \sum_{i=1}^{\infty} \varphi_i(X) q_i(t) \quad (3.2.1)$$

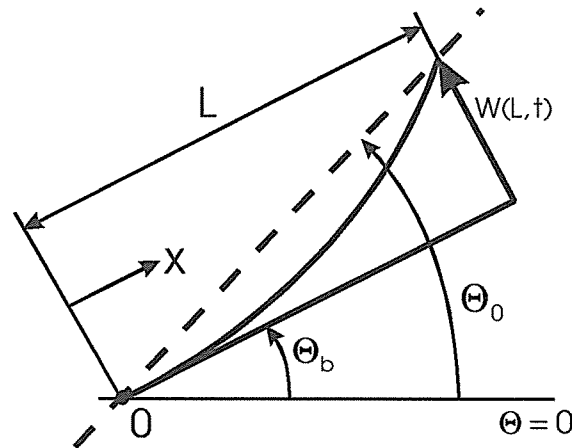


Figure 3.1 Definitions for the flexible beam.

The derivation in Appendix A.1 yields a set of ordinary differential equations for the time depending parts of $W(X,t)$:

$$\omega_n^2 a_n + 2\zeta_n \omega_n \dot{a}_n + \ddot{a}_n = -\alpha_n^* \ddot{\Theta}_b - \sum_{i=1}^{\infty} \beta_{ni}^* \ddot{a}_i \quad (3.2.2)$$

where:

ω_n = eigenmode frequency clamped free beam

ζ_n = eigenmode relative damping coefficient

$$\alpha_n^* = \alpha_n + \frac{m_p \varphi_n(L)}{\mu_n}; \quad \beta_{ni}^* = \frac{m_p \varphi_i(L) \varphi_n(L)}{\mu_n};$$

$$\mu_n = \frac{\rho A L}{4}$$

The index 'n' represents one of the beams infinite number of modes. Because the hubangle Θ_b will be measured and not it's second time derivate, we modify equation 3.2.2 by integrating it twice:

$$\omega_n^2 p_n + 2\zeta_n \omega_n \dot{p}_n + \ddot{p}_n = -\alpha_n^* \Theta_b - \sum_{i=1}^{\infty} \beta_{ni}^* \ddot{p}_i \quad (3.2.4)$$

$$\ddot{p} = q$$

The simulation of the flexible beam behaviour is performed in matrix notation, therefore the differential equation has to be converted to the form:

$$W \underline{p} + R \dot{\underline{p}} + \underline{p} = -\underline{\alpha} \Theta_b - F \ddot{\underline{p}} \quad (3.2.5)$$

where:

$$\underline{p}^T = [p_1, p_2, p_3, \dots]$$

$$W = \begin{bmatrix} \omega_1^2 & 0 & \dots & \underline{0}^T \\ 0 & \omega_2^2 & & \vdots \\ \vdots & & \ddots & \underline{0}^T \\ \underline{0} & \dots & \underline{0} & \omega_n^2 \end{bmatrix}, \quad R = \begin{bmatrix} 2\zeta_1\omega_1 & & \dots & \underline{0}^T \\ & 2\zeta_2\omega_2 & & \vdots \\ \vdots & & \ddots & \underline{0}^T \\ \underline{0} & \dots & \underline{0} & 2\zeta_n\omega_n \end{bmatrix}$$

$$\underline{\alpha}^T = [\alpha_1^*, \alpha_2^*, \alpha_3^*, \dots], \quad F = \begin{bmatrix} \beta_{11}^* & \beta_{12}^* & \dots & \beta_{1n}^* \\ \beta_{21}^* & \beta_{22}^* & & \\ \vdots & & \ddots & \\ \beta_{n1}^* & & & \beta_{nn}^* \end{bmatrix}$$

If we order the term of equation 3.2.5 properly, we obtain:

$$(I+F)\ddot{\underline{p}} + R\dot{\underline{p}} + W\underline{p} = -\underline{\alpha}\Theta_b; \quad \ddot{\underline{p}} = \underline{q} \quad (3.2.6)$$

In this equation for the modal motion \underline{q} the term '(I+F)' represents the influence of a payload in the systems equation (F solely contains B^* terms, which in turn contain the payload m_p). An increase of payload will decrease the eigenmode frequencies of the (clamped free) beam. The "R" term represents the damping coefficients of the eigenmodes. The "W" term contains the square of the eigenmode frequencies. The right-hand term represents the system input i.e. the hub angle Θ_b multiplied by the vector $\underline{\alpha}_n$ that depends on the material and geometrical properties of the link and the mass of the payload.

A modified version of this equation (See appendix C) is used to simulate the behaviour of the flexible beam. Theoretically the dimension of the matrix in equation 3.2.6 is of infinite order ($n \rightarrow \infty$), therefore we have to limit the number of matrix entrances by decreasing the number of modes that are taken into account. This reduction will be carried out later on in this report.

Since we are mainly interested in the position of the end-effector i.e. the payload and $W(X,t)$ only expresses the deflection from the imaginary rigid body (hub-) angle Θ_b , the angle Θ_0 (see figure 3.1) is defined:

$$\Theta_0 = \Theta_b + \frac{W(L,t)}{L} = \Theta_b + \frac{1}{L} \sum_{n=1}^{\infty} \varphi_n(L) q_n(t) = \Theta_b + \frac{1}{L} \sum_{n=1}^{\infty} \varphi_n(L) \ddot{p}_n(t) \quad (3.2.7)$$

The given relation is applicable only if $W(L,t) \ll L$. From now on Θ_0 will be the controlled output of the flexible beam system.

3.3 Actuator model

To actuate the flexible beam a servo motor is used. The assumptions made for the servo motor system are:

- The servo system provides an angular velocity to the flexible beam system
- The servo system can perfectly be modelled by a first order system

The system input is the servo-amplifier input signal u . In Kruse ('90) the following equation for the servo system is given:

$$\dot{\Theta}_b = \frac{K_{PA}}{n(K_m + K_d')} u; \quad \dot{\Theta}_b = K_A u \quad (3.3.1)$$

Where n represents the gear ratio,

$$\begin{aligned} K_m &= \text{Motor constant (Nm/A)} \\ K_{PA} &= \text{Gain of the power amp. (-)} \\ K_d &= \text{Velocity feedback gain (Vs)} \\ K_d' &= \frac{K_{PA}}{n} K_d \end{aligned} \quad (3.3.2)$$

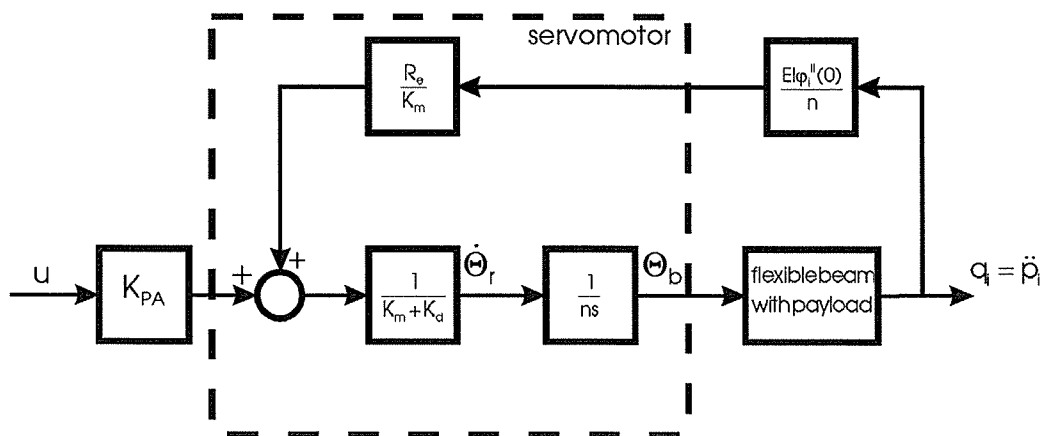


Figure 3.2 block diagram of the servomotor.

We must also account for the torque that the link will impose on the hub, for this will affect the equation of motion of the hub. This is carried out by a feedback loop (see figure 3.2) in

which the feedback torque is represented by the term $\frac{EI\varphi_i''(0)}{n}$. The feedback loop can also be regarded as feedback of the elastic energy present in the flexible beam. The total equation of motion for Θ_b can be obtained from the block diagram of the servomotor (see figure 3.2).

The resulting equation of motion for the hubangle is denoted by:

$$\dot{\Theta}_b = r \sum_{i=1}^{\infty} \varphi_i''(0) \ddot{\rho}_i + K_A u \quad (3.3.3)$$

where:

$$r = \frac{EI R_e}{n^2 K_m (K_m + K_d')} ; K_A = \frac{K_{PA}}{n(k_m + K_d')} ; R_e = \text{Rotor resistance } (\Omega) \quad (3.3.4)$$

When equation 3.3.3 is substituted in equation 3.2.7 the equation of motion for the controlled output Θ_0 is obtained. The state space matrices that are used to simulate the flexible beams behaviour are defined in appendix C.

Chapter 4

Experimental set-up

4.1 Introduction

The freedom in the design process of the experimental set-up was restricted by a number of predetermined conditions. These conditions will be brought up in the following sections. Besides these conditions a number of design demands were stated in the description of the assignment:

1. The experimental set-up will be used to test experimental flexible beam controllers. Besides testing the controller performances, demonstrations must be performed.
2. The experimental set-up should be able to function in a horizontal as well as in a vertical plane. This can demonstrate the performance of controllers that take gravitational forces into account.
3. The set-up should offer possibilities to vary parameters such as the beams Young's modulus or payload. These varying parameters will be used to test adaptive and/or robust controllers.

In the next section the dimensioning of the flexible beam will be considered. The choice of sensors is explained in section 4.3. In section 4.4 the selection of the servomotor/gearbox combination is discussed. Section 4.5 deals with the assembly of all components in the entire set-up.

4.2 Dimensioning of the flexible beam

A design demand for the experimental set-up was that it would be suitable for demonstration purposes. After implementation of the flexible beam controller a spectator should be able to notice the difference between a classical controller and the flexible-beam controller. As the human vision is capable of following oscillating movements up to 20 Hz, the frequency of the first flexible mode must be lower than 20 Hz. To obtain a slowly oscillating beam, the actual frequency is designed to be approximately 5 Hz.

The material of the beam was chosen to be aluminium because of its low Young's modulus. Design demand 2 implies that the plane in which the beam moves can be changed by an operator. This constrains the weight and dimensions of the total set-up. The housing of the total set-up is a steel cube with edges of 400 mm. The weight (gravitational force) of the cube is presumed to invoke enough friction to fix the set-up to its foundation.

Using equation A.2.6. we can calculate the eigenfrequencies of each mode.

$$\omega^2 = \frac{EI}{\rho AL^4} (\gamma L)^4; \quad \omega = 2\pi f \quad (4.2.1)$$

$$L = \sqrt[4]{\frac{EI(\gamma L)^4}{\rho A(2\pi f)^2}} \quad (4.2.2)$$

with:

$$E = 7,0 \cdot 10^{10} \quad [\text{N/m}^2]$$

$$I = 2,5 \cdot 10^{-12} \quad [\text{m}^4]$$

$$\gamma L = 1,87510 \quad [-]$$

$$\rho = 2,7 \cdot 10^3 \quad [\text{Kg/m}^3]$$

$$A = b \cdot h = 3 \cdot 10^{-2} \cdot 1 \cdot 10^{-3} = 3 \cdot 10^{-5} \quad [\text{m}^2]$$

$$f = 5 \quad [\text{Hz}]$$

This results in $L = 405,6$ mm for the length of the beam. The length of the beam is chosen to be 430 mm. This results in the following frequencies of the eigenmodes (unloaded):

Table 4.1. Frequencies of the first five eigenmodes.

i	f_i [Hz]
1	4.4485
2	27.8781
3	78.0594
4	152.9653
5	252.8626

The mass of the beam can easily be derived by:

$$m = \rho AL = 2,7 \cdot 10^3 \cdot 0,03 \cdot 0,001 \cdot 0,43 = 0.03483 \quad [\text{Kg}] \quad (4.2.3)$$

To verify the accuracy of the model presented in Chapter 3, an auto-powerspectrum is calculated from a measured time-domain impulse response. The time-domain signal is generated by an accelerometer and sampled with a frequency of 256 Hz by a bk 2032 (Bruel & Kjaer) signal processing unit. The acceleration signal is printed in figure 4.1.

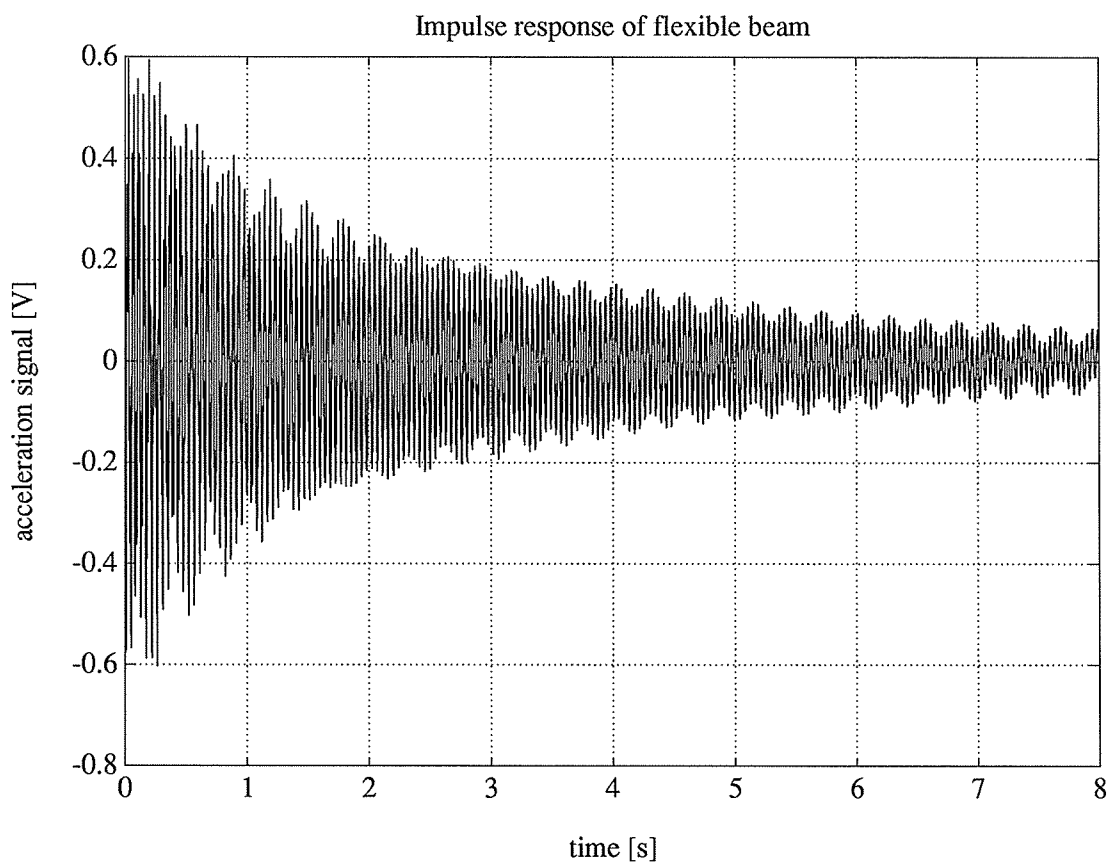


Figure 4.1 Time-domain impulse response.

If we use a hanning window and perform a FFT calculation on the windowed signal, the frequency components of the flexible beam system can be determined. The resulting auto-powerspectrum is printed in figure 4.2.

Since the impulse was invoked by a flick of a fingernail, we don't know the exact frequency contents of the input. Therefore, we can not obtain any absolute values of transfer functions. However the frequencies of the eigenmodes and the damping of these eigenmodes can be retrieved from this measurement. The damping of each mode can be found by filtering the signal from figure 4.1. This filtering is carried out by a fifth order Butterworth filter (see Appendix D). The resulting bandpass filters are tuned to filter out one eigenfrequency. Figure D.2 (Appendix D) shows the first three filtered eigenfrequencies. (The same results were obtained using Kalman filters).

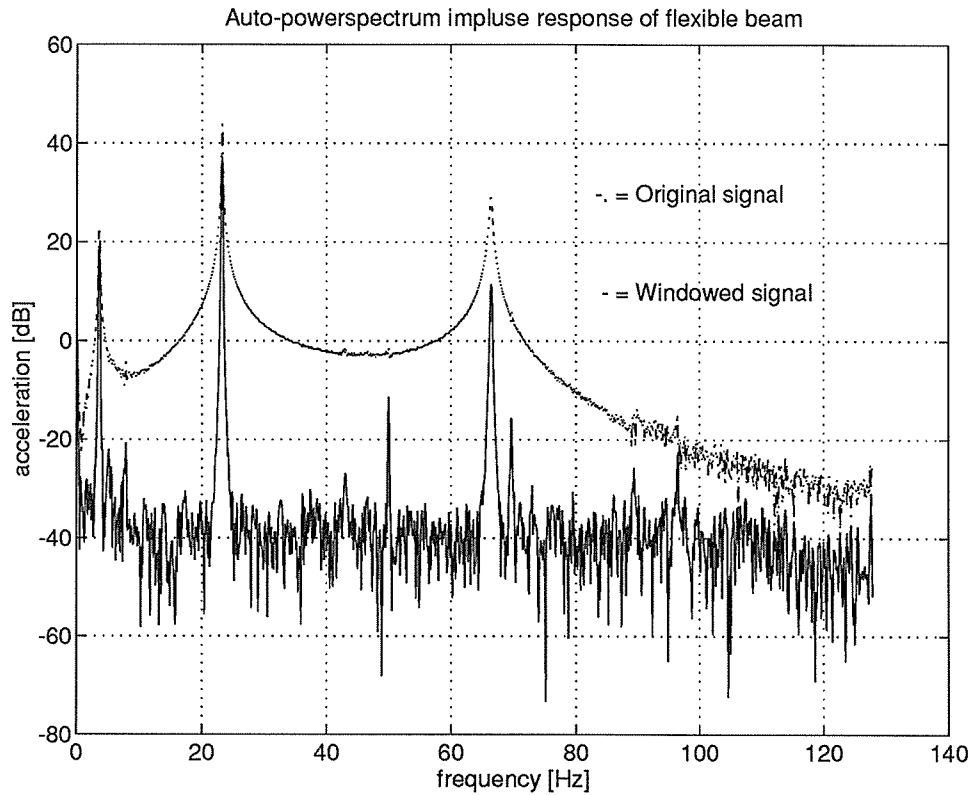


Figure 4.2 Auto-powerspectrum of the flexible beam.

The impulse response of an undercritically damped system can be approximated by the function :

$$q_i(t) = A \cdot \sin(2\pi f_i t + \phi_i) \cdot e^{-t \zeta_i \omega_i} \quad (4.2.4)$$

with $e^{-t \zeta_i \omega_i}$ as the damping term. The value of $\zeta_i \omega_i$ is determined by the exponent of the best matching curve to the amplitude decrease. The damping terms of the first two modes are determined in Appendix D (figure D.3 and D.4). In table 4.1 the first three frequencies of the eigenmodes from figure 4.2 are compared to the calculated values of these modes. The calculated values refer to a beam with an accelerometer (mass: 10 grams) :

Table 4.1 First three eigenmode frequencies

n	f_n (Hz) measured	f_n (Hz) calculated	f_m / f_c (-)	ζ_n (-)
1	3.56	3.92	0.91	0.0019
2	23.6	25.1	0.94	0.0018
3	67.3	71.7	0.94	--

The difference in the calculated frequencies might be explained by a difference in payload. To transport the acceleration signal to its amplifier, a cable is attached to the beam. The mass of this cable can affect the eigenfrequencies of the beam. Also a difference in Young's modulus might explain the difference between the frequencies.

The first eigenfrequency of the unloaded system was designed to be 4.45 (Hz), due to the sensor (acts as payload) this frequency has shifted to 3.56 (Hz). Since the mass of the accelerometer is of the same order as the mass of the beam it would be advisable to investigate sensors-systems that have less influence on the system, for example (piezoelectric) strain-gauges.

4.3 Sensors

One of the conditions of the assignment was that the movements of the beams end were to be measured with accelerometers. At TPD two accelerometers (Bruel & Kjaer) were available, and also the knowledge and the peripheral equipment to operate the sensors were present. To be able to use the accelerometer as an absolute sensor of the acceleration at a certain location on the beam, the accelerometer has to be calibrated. This is done by connecting it to a calibrator that generates an acceleration signal of $10 \text{ (m/s}^2\text{)}$ (RMS). The value measured from the acceleration sensor can now be compared to the calibration value.

Equation 3.2.7 shows that the deflection at each point X on the beam, contains contributions of all modes. The values of $\varphi_i(X)$ (see equation A.1.13) determine the ratio between the maximum contributions (amplitudes). For instance at the location $X=L$ these values equal $-1^{(i+1)}$ (see figure A.4). can be determined by solving equation A.2.23. However, besides the amplitude also the value of the modal motion ($\ddot{q}_i(t)$) is necessary to bring back the acceleration value to the individual contributions of each mode. The measured acceleration signal contains the acceleration due to the deflections of the arm plus the acceleration due to the hub movement ($\ddot{\Theta}_b X_0$) that can be calculated from the measurements of Θ_b . The measured signal can be written as:

$$u_{\text{acc}} = K_{\text{acc}} \left(\frac{\partial^2 W(X_0, t)}{\partial t^2} + \ddot{\Theta}_b X_0 \right) = K_{\text{acc}} \left(\sum_{i=1}^{\infty} \varphi_i(X_0) \frac{\partial^2 q_i(t)}{\partial t^2} + \ddot{\Theta}_b X_0 \right) \quad (4.3.1)$$

where:

u_{acc} = voltage accelerometer system
 K_{acc} = amplifier constant
 X_0 = position accelerometer

In matrix form equation 4.3.1 can be written as:

$$\underline{u}_{\text{acc}} = D \ddot{\underline{q}} - K_{\text{acc}} \ddot{\underline{\Theta}}_b \underline{X}_0 \quad (4.3.2)$$

where:

$$\begin{aligned} \underline{X}_0^T &= [X_1, X_2, \dots] \\ \underline{u}_{\text{acc}}^T &= [u_{\text{acc}}(X_1, t), u_{\text{acc}}(X_2, t), \dots] \\ D_{ij} &= K_{\text{acc}} \varphi_j(X_i) \\ \underline{\ddot{q}}^T &= [\ddot{q}_1, \ddot{q}_2, \dots] \end{aligned}$$

Now we can calculate the modal modes contributions from the measurements $\underline{u}_{\text{acc}}$ by inverting the decoupling matrix "D":

$$\underline{\ddot{q}} = D^{-1} (\underline{u}_{\text{acc}} - K_{\text{acc}} \ddot{\underline{\Theta}}_b \underline{X}_0) \quad (4.3.3)$$

This method will be referred to as the decoupling of the accelerometer signals. Because of the inversion of matrix D the number of accelerometers must be equal to the number of modes that one wants to disentangle.

In chapter 3 it was already mentioned that theoretically the number of modes is infinite. This implies that an infinite number of accelerometers should be installed. Of course this is an impracticable task. Due to the limited bandwidth of our servo system (see section 4.4) higher modes will hardly be excited. Furthermore these higher modes damp out fast. In our case this results in a concentrated attention to the lowest modes for our controller design. The number of accelerometers to install is limited by the two input channels of the DSP. One channel will be used to measure the shaft position, which leaves one input channel to measure the acceleration at one location on the beam. At the free end of the beam at $X = 430$ (mm) ($X = L$) all modes have a contribution unequal to zero. If we eventually want to use the information of all present modes we must locate our sensor at $X = L$. Since we can only measure one acceleration and are interested in the lowest mode, we must treat the contributions of the higher modes as measurement noise. The disturbing effect of higher modes can be decreased in two ways. The first method is to position the accelerometer at

a location where the contribution of the closest higher mode equals zero. These locations can be calculated by solving X from equation A.2.23 with a zero left hand term. The second method is to make the system closed loop response slower than the disturbing modes. This ensures that disturbing higher modes will not be amplified and finally damp out. The second method can be implemented by inserting a suitable filter in the control loop (see figure 4.4).

Since equation 3.2.8, defining the controlled output, contains the position and not the acceleration, the acceleration signal has to be transformed into a position signal. Integrating the acceleration signal twice, the position signal could be obtained. However, because we are only dealing with position control and a linear model, q_i can also be determined analytically. From equation 3.2.6 follows that the free response of the beam is an oscillation:

$$\begin{aligned} \ddot{q}_i &= A \sin(\omega_i t + \phi_i) \\ q_i &= -\frac{A}{\omega_i^2} \sin(\omega_i t + \phi_i); \quad q_i = -\frac{1}{\omega_i^2} \ddot{q}_i \end{aligned} \quad (4.3.4)$$

ω_i^2 equals the angular velocity of the modal motion and is calculated in section 4.2. The calculation is carried out by the control algorithm in the DSP and yields the modal motion position q_i that is used for the feedback loop.

Our flexible beam controller also requires measurement of the shaft position. The restriction of the shaft-position sensor was that it should supply an analog signal. This analog signal was necessary to comply with the input standard of the DSP units ("Stochi" and "Octopus") used by the Active Noise Control department. One way to obtain such an analog signal was to use an advanced servo system (with position control). However these systems generally make use of non standard programming languages. Additionally the system analysis is complicated by the indistinct control loop inside the servo system. A second more easy, clearly less expensive solution is the application of a precision potentiometer. When the potentiometer is connected to a power supply, and its tuning axis is attached to the rotation axis of the beam the output voltage of the potentiometer is linear in the axis position (shaft position).

Technical data of the sensors can be found in Appendix F.

4.4 Servomotor

To actuate the flexible beam a servo system is selected. The most important selection criteria were:

- small mechanical time constant
- small electrical time constant
- good low speed behaviour

Since it is our intention to implement computed torque (model based) controllers we must have a full description of the servo system. Unlike the inertia terms, that are very accurately given by the manufacturer, we know almost nothing about the friction within the servo system. The manuals only give maximum values of the friction but do not mention whether this is Coulomb- or viscous friction. This subject should be handled in future research.

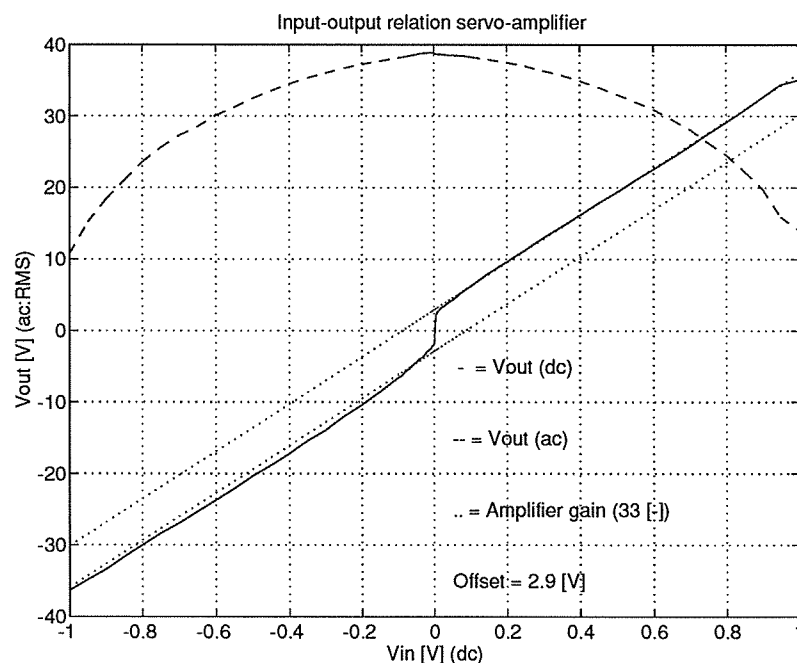


Figure 4.3 Servo amplifier gain.

After assembly of the different modules, the linearity of the servo-amplifier was measured. This can be done by uncoupling the servomotor and measuring the output voltage as a result of a varying input voltage. The measured values are put together in figure 4.3 to visualise the input-output relation of the amplifier.

Because the implemented controller is based on linear servo system theory, the influence of the non linear relation shown in figure 4.3 should be investigated. The controllers implemented on the system don't account for any servo system non-linearity yet.

In section 3.3 the relation for our servo system was given:

$$\dot{\Theta}_b = K_A u \quad (4.4.1)$$

To use this equation in the control design and the simulations the value of K_A must be known. The servo system manufacturer gives for K_A the value $50 \text{ (rpm/V)} = 7.96 \text{ (rad/s/V)}$. However this value has not yet been determined experimentally and therefore it is set to '1' during simulations. The real value of K_A can be determined by measurement of the relation between the angular velocity $\dot{\Theta}_b$ and the input voltage of the servo amplifier.

Technical data of the servomotor and gearbox can be found in Appendix F

4.5 Composition of the set-up

The control loop is completed by a DSP board inside a PC. It's characteristics are summarized in Appendix F. This processor board must be programmed in C. A major disadvantage of this DSP is that up to now it can only be controlled by a "debugger" that operates under MS-Windows.

The overview of the entire experimental set-up is displayed in figure 4.4.

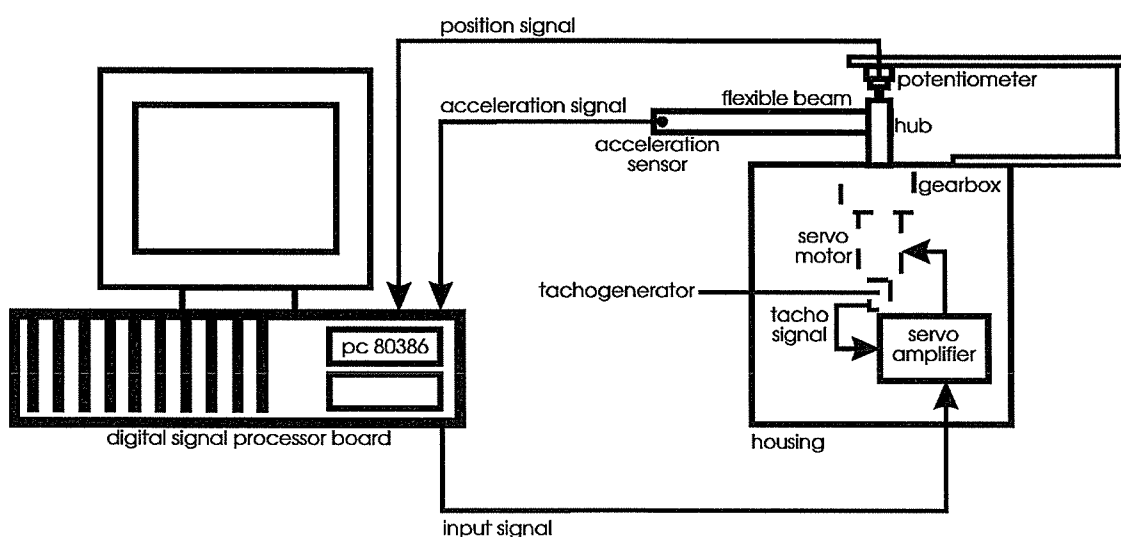


figure 4.4 Schematic overview of the experimental set-up.

Chapter 5

Controller design for a flexible beam

5.1 Introduction

Since the main goal of this report is to design an experimental set-up to illustrate the possibilities of flexible beam control, the controllers implemented are not really advanced. This is mainly due to the restriction of time. However in the long term other, more advanced controllers should be implemented. Other restrictions, like the number of in- and output signals, constrained the number of eigenmodes to be controlled. The PD-controller that will be discussed in section 5.2 will not deal with the flexibility of the beam. The output-feedback controller in section 5.3 is designed to damp out the deflections resulting from the beam flexibility. Both a reduced output-feedback (although two modes are simulated, only one mode is controlled) and a full output-feedback are regarded. In all cases the input signal (desired shaft position; dsp) used for the simulations is a step at $t = 0$ of magnitude $\pi/4$ (rad)

5.2 P-controller

In this section only the P-action of this controller will be discussed. The D-action is already realized within the servo system. Although this will not be explicitly stated, the velocity feedback loop will also be applicable for the controllers discussed in the next sections.

The tuning for the controller must yield a minimal rise time, furthermore the control action may not result in an input saturation (maximum: 1 (Volt)) of the servo amplifier. Figure 5.1 gives a block scheme for the PD-controller

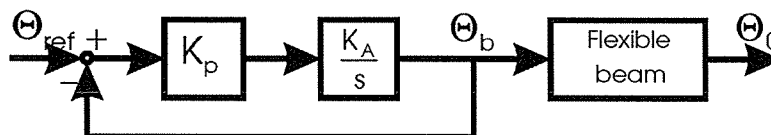


Figure 5.1. P-controller

Since only the difference between the desired shaft position of $\pi/4$ (rad) and the actual position determines the input signal, the highest input signal will be found at $t = 0$ sec. From the first order differential equation 3.3.1 follows that the resulting input signal will be a

negative e-power (first order step response). We obtain a maximum input signal of 1 Volt if we tune the controller gain (K_p) to the inverse of the maximum difference ($K_p=1/dsp$). This strategy implies that a new control gain must be calculated for different step sizes. This however can easily be done by the control algorithm in the DSP.

5.3 Output-Feedback controller

This controller is tuned to obtain minimal rise time, but also to provide maximum damping for the flexible modes. The control actions may not result in input saturation ($u \leq 1$ Volt).

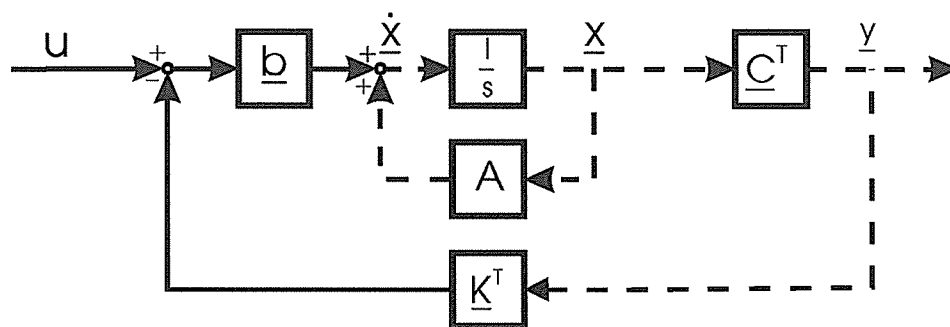


Figure 5.2 Block scheme of the controller.

Note that the dashed lines in figure 5.2 symbolise multi variable signals.

The value of K_1 is determined by an iterative process of trial and error which yields $K_1 = 30$ (-) as the maximum feedback gain for the first mode. For the full output-feedback controller, two controller parameters must be set. Since we only have the maximum input voltage criterion, we must invent a second criterion to be able to set both parameters. The second criterion will be:

$$\frac{K_1}{K_2} \cong 1 \quad (5.3.1)$$

This implies that although in absolute sense position errors due to one of the modes will result in equal control efforts, the first mode will have the highest relative damping. This can be derived from the definition of the relative damping coefficient ζ_i :

$$e^{-t\zeta_i\omega_i} \quad (5.3.2)$$

$$\zeta_i\omega_i = \lambda_i \quad (5.3.3)$$

$$\lambda_i = \text{eigenvalue of } [A - b * k_f * C] \quad (5.3.4)$$

$$k_f = [K_p \quad K_1 \quad K_2 \quad 0] \quad (5.3.5)$$

The initial value of K_1 and K_2 is 15. After several simulations, the values $K_1=12$ and $K_2=17$

show to result in a maximum input of 1 Volt. The resulting relative damping terms follow from the real part of the eigenvalues of the controlled system matrix. Table 5.1 provides an overview for the relative damping terms of the uncontrolled, the reduced output-feedback and the full output-feedback situation.

Table 5.1 Damping terms overview

n	ζ_n (-)	ζ_n (-) (red.)	ζ_n (-) (full)
1	0.0019	2.348	0.95
2	0.0018	0.0018	0.09

5.4 Simulations

This section displays the results of the simulations with a PD-controller, a reduced output-feedback controller and a full output-feedback controller. Figure 5.3 shows the PD-controller simulation. Figure 5.4 shows the results of a reduced output-feedback controller (the lowest of two simulated modes is controlled). Figure 5.5 shows the results of a full output-feedback controller.

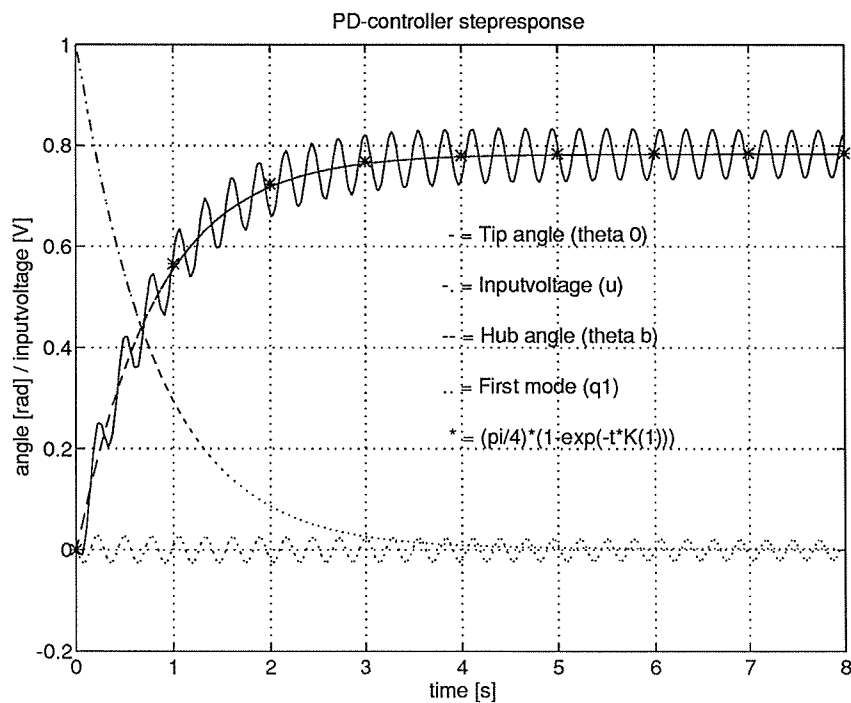


Figure 5.3

Figure 5.3 clearly shows a first order step response for the hub angle Θ_b combined with a second order damped oscillation for the eigen modes. Also the non-minimum phase behaviour is visible as the beams tip angle Θ_0 first moves in the opposite step direction.

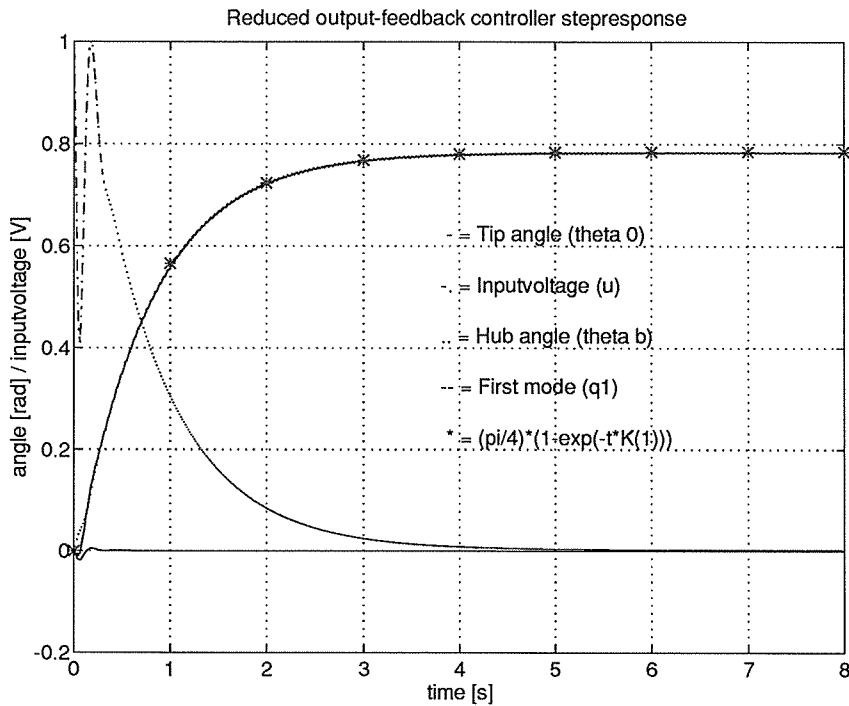


Figure 5.4

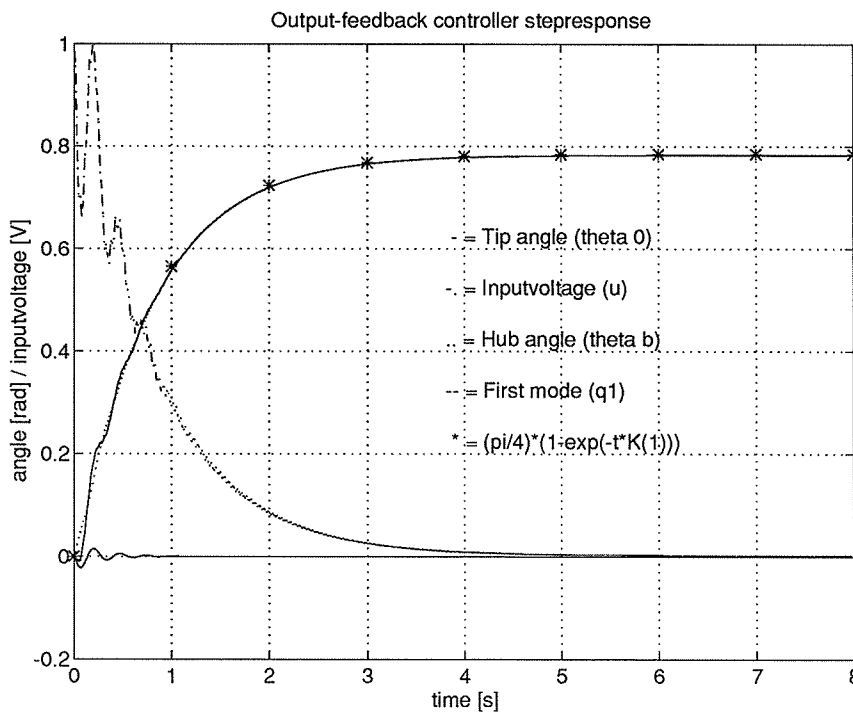


Figure 5.5

Figure 5.4 shows a very fast damping of the first eigenmode, but it still holds a ripple resulting from an uncontrolled second mode. Due to the extra contribution of the second eigenmode to the control input, the first mode in figure 5.5 can not be damped out as fast as in the previous case, but the ripple due to the second mode is no longer visible. This implies that the beams tip can be positioned with higher accuracy. Depending on the time constants of the servo system the higher modes can be controlled to minimise their contribution to the tip position.

5.5 Experiments

Because at the time this report was written, it was not yet possible to communicate (exchange information) with the DSP board, a performance measurement of the implemented controller was not possible. To demonstrate the effect of the controller the beam is positioned at a certain angle and excited by a flick of a fingernail or hand. The demonstration clearly showed that once the controller is turned on, the oscillations damp out within a second. Whereas without controller the oscillations persist for longer than half a minute.

Chapter 6

Conclusions

In this report the realisation of an experimental flexible beam set-up is described. A literature review as well as a controller design of a relatively simple output-feedback controller are shown.

Literature presents different models for a flexible beam system. The modelling used in this report contains several linear approximations and therefore it will not be valid under all conditions, for instance at high speed conditions. The literature review shows that although a lot of research is done on flexible beam controllers, the computed torque controllers seldom have a practical implementation. This in spite of the promising performance on trajectory control of this type of controller; In general the authors state that the performance of computed torque controllers is superior to the performance of output feedback controllers.

In the case of position control the presented output feedback controller suppresses the occurring oscillations very good. To obtain the highest position accuracy, a maximum number of modes should be controlled. However because of the square decoupling matrix (sensor signals are decoupled to individual mode contributions), we should use at least the same number of sensors as modes to be controlled.

Our experimental set-up uses an accelerometer to detect the first mode. The mass of this sensor is of the same order as the mass of the beam and therefore the sensor has a large (undesired) influence on the beams behaviour. One sensor at the tip of the beam can easily be modelled as a payload carried by the arm. However if we increase the number of sensors, and place them at various locations along the beam, the modelling will increase in complexity as well.

Recommendations

Because the performance of computed torque controllers described in literature is said to be superior to that of output feedback controllers, they should be implemented and tested on the experimental set-up. In that way we can compare the performances of different

types of controllers and find out which one is the most suited for practical implementation of trajectory control.

Since it is our intention to implement different model based controllers, it will be fruitful to obtain a highly accurate model of our system. For instance, the measured non linear behaviour of the servo-amplifier and its influence on the linearity of the total servo system must be investigated. Also the influence of friction in the system should be investigated. The parameters of the friction model can be determined by measurements on the system.

In the preset set-up the accelerometer has a relatively large influence on the beam system, therefor it might be wise to investigate other ways of mode detection. The best solution would be to find a way of mode detection whose influence on the model can be neglected (contactless optical measurement or piezoelectric strain gauges).

Bibliography

- ABB survey on robotisation today: applications, issues and expectations in Belgium and the Netherlands. Edited by R van Keilegom from a survey conducted by the Roland Berger Forschungs-Institut für Markt- und Systemforschung, Munchen, Germany. 1992.
- Bayo, E. An inverse dynamics based closed loop trajectory tracking control for a flexible beam. ASME the annual winter meeting of the ASME, Atlanta, Georgia. pp.21-26. 1991
- Berghuis, H. Model based Robot Control: from Theory to Practice. Ph.D. Thesis University of Twente. 1993.
- Book, W. J. Tracking control of a non-minimum phase flexible manipulator. ASME the annual winter meeting of the ASME, Atlanta, Georgia. pp 27-35. 1991.
- Drent, K. H. Implementation of a flexible link model in a designed robotsystem, using the finite element methode. 1988.
- Fraser, A.R. Pertubation techniques for flexible manipulators. 1991.
- Heijman, D. Control of a flexible link. Master's Thesis Eindhoven university of thechnology, the Netherlands. 1993.
- Henrichfreise, H. Aktive schwingungsdämpfung an einem elastischen knickarmroboter. Braunschweig/ Wiebaden, Germany. 1987.
- Kinsler, L.E. et al. Fundamentals of acoustics, third edition. John Wiley & Sons, Inc. pag 57-77. 1982
- Kruse, I. Modelling and control of a flexible beam and robotarm. Ph.D. Thesis University of Twente, the Netherlands. 1990.
- Lammerts, I. Adaptive computed reference computed torque control of flexible manipulators. Ph.D. Thesis Eindhoven University of technology, the Netherlands. 1993.

- Lucassen, F. Modelleringsalgoritmen voor Industriële robots. Ph.D. Thesis Eindhoven University of technology, the Netherlands. 1990.
- Meirovitch, L. Elements of vibration analysis, second edition. McGraw-Hill Inc. pag 281-285.1986.
- Ouchi ,S. et al. Active vibration control of a motor system by H_{∞} control. 1992

Appendix A

A.1 Flexible beam model

In figure A.1 the forces and moments on a beam element P are drawn. To simplify the derivation the gravity terms are omitted and all mass of the beam is concentrated on the beam axis.

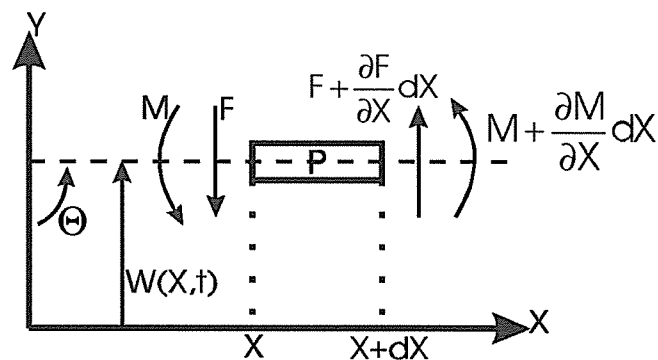


Figure A.1. Force balance of a beam element

$W(X,t)$ stands for the deflection of the neutral axis of the originally straight beam. From the balance of the bending moments follows:

$$F(X,t) = -\frac{\partial M(X,t)}{\partial X} \quad (\text{A.1.1})$$

From the bending theory of Timoschenko follows:

$$M(X,t) = -EI \frac{\partial^2 W(X,t)}{\partial X^2} \quad (\text{A.1.2})$$

with Young or elasticity modulus E and area moment of inertia I .

with A.1 for F follows:

$$F(X,t) = EI \frac{\partial^3 W(X,t)}{\partial X^3} \quad (\text{A.1.3})$$

Applying Newton's law to the beam element results in:

$$\frac{\partial F(X,t)}{\partial X} = \rho A \ddot{Y} \quad (\text{A.1.4})$$

with specific mass ρ and cross-section area A

To describe the vibrations of the beam we need a co-ordinate frame as shown in figure A.2.

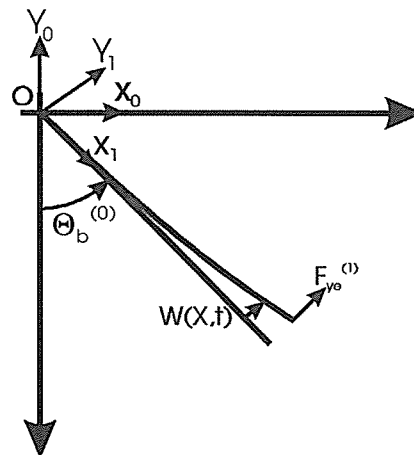


Figure A.2. Co-ordinate frames used in the modelling

The superscripts refer to the co-ordinate frames X_0, Y_0 and X_1, Y_1 that represent the co-ordinate frame fixed to the origin and the body attached frame respectively. We assume that the rotation axis of the beam is fixed in the origin. The angle between the two co-ordinate frames is represented by Θ_b . This angle might also be referred to as the hub angle.

Acceleration of a beam element, perpendicular to the beam axis, will be denoted by:

$$\ddot{Y}_1 = X \cdot \ddot{\Theta}_b + \ddot{W} - W \cdot (\dot{\Theta}_b)^2 \quad (\text{A.1.5})$$

At this point we introduce terms concerning the occurring damping forces. Kruse ('90) uses the following terms:

$$\delta_E \frac{\partial W}{\partial t} + \delta_I \frac{\partial^5 W}{\partial X^4 \partial t} \quad (\text{A.1.6})$$

According to Ray ('78); the first term represents the damping due to air friction, and the second the damping due to the internal energy losses. However there is still a lot of research to be done on the damping since there are no exact values mentioned for the terms δ_E and δ_I . In our case the damping that will be provided by the controller is much larger than the damping for the lowest mode.

When equation (3) and (5) are combined with equation (4) and the damping terms, the following result is obtained:

$$EI \frac{\partial^4 W}{\partial X^4} + \rho A \frac{\partial^2 W}{\partial t^2} + \delta_E \frac{\partial W}{\partial t} + \delta_I \frac{\partial^5 W}{\partial X^4 \partial t} = \rho A (X \ddot{\Theta}_b - W (\dot{\Theta}_b)^2) + \delta(x-L) F_{ye}^{(1)}; \\ W = W(X,t) \quad (\text{A.1.7})$$

The term $W(\dot{\theta}_b)^2$ from equation A.1.7 will be disregarded since in the set-up $(\dot{\theta}_b)^2 \ll \omega_1^2$, where ω_1 is the lowest eigenmode frequency of the beam. The force $F_{ye}^{(1)}$ is introduced (see figure A.2) in the equation which represents the force a payload would impose on the beam. Since the equation A.1.7 is valid for the entire beam and $F_{ye}^{(1)}$ only acts at the end of the beam ($X=L$) the Dirac function $\delta(X-L)$ is added.

To solve the differential equation A.1.7 we must define boundary conditions. Basically the beam is modelled as clamped free, but here we will restrict the degrees of freedom at the side of the beam where the driving force is situated. This yields:

$$W(0,t) = 0 \quad (\text{A.1.8})$$

$$\frac{\partial W(X,t)}{\partial X} \Big|_{x=0} = 0 \quad (\text{A.1.9})$$

The other end is free and therefor the force $F(X,t)$ and the bending moment $M(X,t)$ are zero at $X = L$. This yields:

$$(\text{A.1.10})$$

$$\frac{\partial^2 W(X,t)}{\partial X^2} \Big|_{x=L} = 0$$

$$\frac{\partial^3 W(X,t)}{\partial X^3} \Big|_{x=L} = 0 \quad (\text{A.1.11})$$

Note that with the presence of a payload the right-hand side of equation A.1.11 is unequal to zero. In the derivation of Kruse, however the eigenfunctions resulting from boundary condition A.1.11 are used for the loaded beam situation aswel.

In order to transform the fourth order partial differential equation into a finite set of ordinary differential equations, the solution to equation A.1.7 is split up into a position depending part and a time depending part.

$$W(X,t) = \sum_{i=1}^{\infty} \varphi_i(X) q_i(t) \quad (\text{A.1.12})$$

The functions $\varphi_i(X)$ (derived in Appendix A.2) equal the clamped free modal modes of the beam, and have the following properties:

$$\varphi_i(L) = (-1)^{i+1} \quad (\text{A.1.13})$$

$$\int_0^L \varphi_i(X) \varphi_j(X) dX = 0 \quad i \neq j \quad (\text{A.1.14})$$

$$\frac{EI}{\rho A} \frac{d^4 \varphi_i(X)}{dX^4} = \omega_i^2 \varphi_i(X); \quad \omega_i^2 = -\frac{\ddot{q}(t)}{q(t)} \quad (\text{A.1.15})$$

Property A.1.14 means that modal modes are orthogonal, this is proven by Kruse ('90).

Property A.1.15 is derived in Appendix A.2

When equation (A.1.13) is substituted in equation (A.1.7) the partial differential equation is transformed into an infinite set of ordinary differential equations. This yields:

$$\sum_{i=1}^{\infty} \omega_i^2 \varphi_i \dot{q}_i + \sum_{i=1}^{\infty} 2\zeta_i \omega_i \varphi_i \dot{q}_i + \sum_{i=1}^{\infty} \varphi_i \ddot{q}_i = -X \ddot{\Theta}_b + \frac{\delta(X-L)}{\rho A} F_{ye} \quad (\text{A.1.17})$$

where:

$$\zeta_i = \frac{\delta_E}{2\rho A \omega_i} + \frac{\delta_i \omega_i}{2\rho A} \quad (\text{A.1.18})$$

To eliminate the "X" terms the equation A.1.17 is integrated over "X" and multiplied by φ_n . This transformation is described in appendix B.1 The resulting ordinary equations are given by:

$$\omega_n^2 \dot{q}_n + 2\zeta_n \omega_n \dot{q}_n + \ddot{q}_n = -\alpha_n \ddot{\Theta}_b + \frac{\varphi_n(L) F_{ye}}{\mu_n} \quad (\text{A.1.19})$$

where:

$$\alpha_n = \frac{\int_0^L X \varphi_n(X) dX}{\int_0^L \varphi_n^2(X) dX}; \quad \mu_n = \rho A \int_0^L \varphi_i^2(X) dX = \frac{\rho A L}{4} \quad (\text{A.1.20})$$

Up to now the influence of a payload m_p has not been cleared. We need to define the acceleration $\ddot{y}_m^{(1)}$, this the acceleration perpendicular to the beams axis, $\ddot{y}_m^{(1)}$ is defined by:

$$\ddot{y}_m^{(1)} = L \ddot{\Theta}_b^{(0)} + W(L, t) = L \ddot{\Theta}_b^{(0)} + \sum_{i=1}^{\infty} \varphi_i(L) \ddot{q}_i(t) \quad (\text{A.1.21})$$

In figure A.3 a flexible beam with payload is shown.

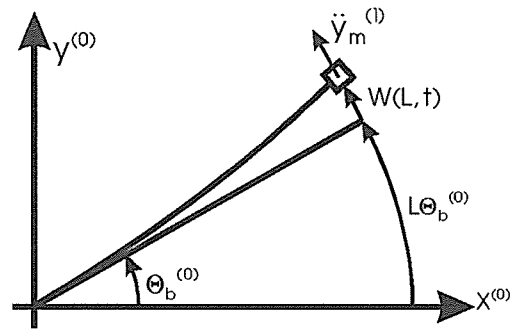


Figure A.3 Flexible beam with payload

The force F_{ye} that is applied perpendicular to the beams end is defined by:

$$F_{ye}^{(1)} = -m_p \ddot{y}_m^{(1)} = -m_p \left(L \ddot{\theta}_b^{(0)} + \sum_{i=1}^{\infty} \varphi_i(L) \ddot{q}_i(t) \right) \quad (\text{A.1.22})$$

Equation A.1.22 is substituted in equation A.1.19 which yields:

$$\omega_n^2 q_n + 2\zeta_n \omega_n \dot{q}_n + \ddot{q}_n = -\alpha_n \ddot{\theta}_b - \sum_{i=1}^{\infty} \beta_{ni} \ddot{q}_i; \quad (\text{A.1.24})$$

$$\alpha_n = \alpha_n + \frac{m_p \varphi_n(L)}{\mu_n}; \quad \beta_{ni} = \frac{m_p \varphi_i(L) \varphi_n(L)}{\mu_n}; \quad \mu_n = \frac{\rho AL}{4} \quad (\text{A.1.25})$$

Equation A.1.24 will be the basic equation for the derivation of our flexible beam model in section 3.2.

A.2 Derivation of $\varphi(X)$

In this section a relation for the modal motions $\varphi(X)$ used in Appendix A.1 is derived. Disregarding shear deformation and rotation of beam elements, Timoshenko's beam equation reduces to the so-called Euler Bernoulli equation for a beam:

$$EI \frac{\partial^4 W}{\partial X^4} + \rho A \frac{\partial^2 W}{\partial t^2} = 0 \quad (\text{A.2.1})$$

This equation can be solved by separation of variables. For that purpose $W(X,t)$ is written as:

$$W(X,t) = \varphi(X)q(t) \quad (\text{A.2.2})$$

Substituting equation A.2.2 into equation A.2.1 and dividing it by $W(X,t)$ yields:

$$\frac{\ddot{q}(t)}{q(t)} = \frac{EI\varphi^{IV}(X)}{\rho A\varphi(X)} \quad (\text{A.2.3})$$

where:

$$\varphi^{IV} = \frac{d^4\varphi(X)}{dX^4} \quad (\text{A.2.4})$$

and:

$$\ddot{q}(t) = \frac{d^2q(t)}{dt^2} \quad (\text{A.2.5})$$

In equation A.2.3 the left hand side depends on t only while the right-hand side depends on X . This results in both sides being equal to the constant $-\omega^2$. The resulting ordinary differential equations are:

$$\ddot{q}(t) = -\omega^2 q(t); \quad \omega^2 = \frac{EI}{\rho A} \gamma^4 \quad (\text{A.2.6})$$

$$\varphi^{IV} = \gamma^4 \varphi(X) \quad (\text{A.2.7})$$

To obtain a solution to the differential equation (A.2.7), the following substitution is used:

$$\varphi_n(X) = Ce^{\lambda X} \quad (\text{A.2.8})$$

where C and λ are constants. After substitution, this results in:

$$\lambda^4 = \gamma^4 \Rightarrow \lambda^2 = \pm\gamma^2 \Rightarrow \lambda = \pm\gamma, \pm j\gamma \quad (\text{A.2.9})$$

With the solutions of equation A.2.7 the eigenfunctions of the beam can be written as:

$$\varphi(X) = c_1 \cosh \gamma X + c_2 \sinh \gamma X + c_3 \cos \gamma r + c_4 \sin \gamma r \quad (\text{A.2.10})$$

where c_1, \dots, c_4 are integration constants. To calculate the values of c_1, \dots, c_4 we need to define the boundary conditions of a clamped free beam. These boundary conditions are (see equations A.1.8-11):

$$\varphi(0) = 0 \quad (\text{A.2.11})$$

$$\varphi'(X)|_{X=0} = 0 \quad (\text{A.2.12})$$

$$\varphi''(X)|_{X=L} = 0 \quad (\text{A.2.13})$$

$$\varphi'''(X)|_{X=L} = 0 \quad (\text{A.2.14})$$

L represents the length of the beam. Substituting equation A.2.10 into equations A.2.11-14 yields:

$$c_1 + c_3 = 0 \quad (\text{A.2.15})$$

$$\gamma(c_2 + c_4) = 0 \quad (\text{A.2.16})$$

$$\gamma^2(c_1 \cosh \gamma L + c_2 \sinh \gamma L - c_3 \cos \gamma L - c_4 \sin \gamma L) = 0 \quad (\text{A.2.17})$$

$$\gamma^3(c_1 \sinh \gamma L + c_2 \cosh \gamma L + c_3 \sin \gamma L - c_4 \cos \gamma L) = 0 \quad (\text{A.2.18})$$

A non trivial solution to these equations is:

$$\cosh \gamma L \cos \gamma L = -1, \quad c_1 = -c_3 \quad \text{and} \quad c_2 = -c_4 \quad (\text{A.2.19})$$

The first equation in A.2.19 is known as the frequency equation (Meirovitch, 1967). Numerical solutions of this equations are given in table A.1.

Table A.1 Numerical solutions to the frequency equation.

i	$\gamma_i L$
1	1.87510
2	4.69409
3	7.85476
4	10.99554
5	14.13717
6	17.27876

The values of $\gamma_i L$ were calculated with the Matlab sub-routine `gammi.m` which is listed in appendix E. The frequency equation has more than one solution. The solutions indexed with "i" are all eigenfunctions of the beam system. Up to now the values of c_1, \dots, c_4 only could be expressed relatively to each other. If we apply property A.1.13:

$$\varphi_i(L) = (-1)^{i+1} \quad (\text{A.2.20})$$

This results in the following absolute values of c_1, \dots, c_4 :

$$c_{i1} = -c_{i3} = \frac{1}{2} \quad (\text{A.2.21})$$

and

$$c_{i2} = -c_{i4} = -\frac{1}{2} \frac{\cos \gamma_i L + \cosh \gamma_i L}{\sin \gamma_i L + \sinh \gamma_i L} \quad (\text{A.2.22})$$

c_{i2} is calculated for some values of "i" in table A.2

Table A.2 some values of c_{i2}

i	c_{i2}
1	-0.367048
2	-0.509234
3	-0.499612
4	-0.500017
5	-0.500000
.	.
.	.
∞	-0.5

To calculate these values a program is written called `ci.m` which is listed in appendix E. The values of c_{i2} lead to a general description of $\varphi(X)$:

$$\varphi_i(X) = c_{i1} (\cosh \gamma_i X - \cos \gamma_i X) + c_{i2} (\sinh \gamma_i X - \sin \gamma_i X) \quad (\text{A.2.23})$$

The first three eigenfunctions according to A.2.23 ($i = 1, 2, 3$) are plotted in figure A.4.

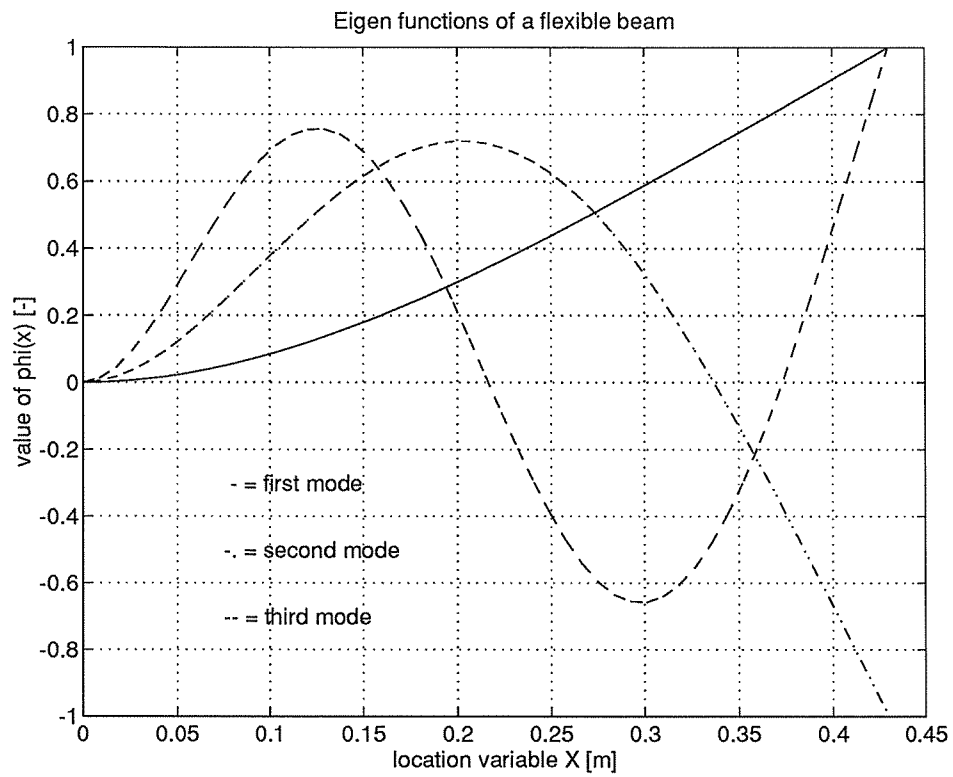


Figure A.4 the first three eigenfunctions of the flexible beam model.

Appendix B

B.1 Differential equation transformation

In appendix A.1 a set of ordinary differential equations was derived. The part depending on "X" will be removed by multiplying it by the eigenfunction φ_n and integrating the resulting equation over "X". This is done one term at a time. The differential equations are given by:

$$\sum_{i=1}^{\infty} \omega_i^2 \varphi_i q_i + \sum_{i=1}^{\infty} 2\zeta_i \omega_i \varphi_i \dot{q}_i + \sum_{i=1}^{\infty} \varphi_i \ddot{q}_i = -X \ddot{\theta}_b + \frac{\delta(X-L)}{\rho A} F_{ye} \quad (\text{B.1.1})$$

Transformation of the first term on the left-side yields:

$$\begin{aligned} \sum_{i=1}^{\infty} \omega_i^2 \varphi_i q_i &\Rightarrow \int_0^L \varphi_n(X) \sum_{i=1}^{\infty} \omega_i^2 \varphi_i(X) q_i(t) dX = \\ &\sum_{i=1}^{\infty} \omega_i^2 q_i(t) \int_0^L \varphi_n(X) \varphi_i(X) dX \end{aligned} \quad (\text{B.1.2})$$

The integration over "X" in equation B.3 is reduced to the multiplication of two eigenfunctions. Due to property A.1.15 the solution is unequal to zero if "i" equals "n". Applying this property yields:

$$\omega_n^2 q_n(t) \int_0^L \varphi_n^2(X) dx \quad (\text{B.1.3})$$

Transformation of the second term on the left-hand side yields:

$$\begin{aligned} \sum_{i=1}^{\infty} 2\zeta_i \omega_i \varphi_i \dot{q}_i &\Rightarrow \int_0^L \varphi_n(X) \sum_{i=1}^{\infty} 2\zeta_i \omega_i \varphi_i(X) \dot{q}_i(t) dX = \\ &\sum_{i=1}^{\infty} 2\zeta_i \omega_i \dot{q}_i(t) \int_0^L \varphi_n(X) \varphi_i(X) dX \end{aligned} \quad (\text{B.1.4})$$

Applying property A.1.15 yields:

$$2\zeta_n \omega_n \dot{q}_n(t) \int_0^L \varphi_n^2(X) dX \quad (\text{B.1.5})$$

Transformation of the third term yields:

$$\sum_{i=1}^{\infty} \varphi_i \ddot{q}_i \Rightarrow \int_0^L \varphi_n(X) \sum_{i=1}^{\infty} \varphi_i(X) \ddot{q}_i(t) = \sum_{i=1}^{\infty} \ddot{q}_i(t) \int_0^L \varphi_n(X) \varphi_i(X) dX \quad (\text{B.1.6})$$

Applying property A.1.15 yields:

$$\ddot{q}_n(t) \int_0^L \varphi_n^2(X) dX \quad (B.1.7)$$

The same transformation is carried out with the right-hand side terms. For the first right-hand side term this yields:

$$-X\ddot{\Theta}_b \Rightarrow -\int_0^L \varphi_n(X) X \ddot{\Theta}_b dX = -\ddot{\Theta}_b \int_0^L \varphi_n(X) X dX \quad (B.1.8)$$

Transformation of the second right-hand side term yields:

$$\begin{aligned} \frac{\delta(X-L)}{\rho A} F_{ye} &\Rightarrow \int_0^L \varphi_n(X) \frac{\delta(X-L)}{\rho A} F_{ye} dX = \\ \frac{F_{ye}}{\rho A} \int_0^L \delta(X-L) \varphi_n(X) dX &= \frac{\varphi_n(L) F_{ye}}{\rho A} \end{aligned} \quad (B.1.9)$$

When all terms of equation B.1 are replaced with their transformed equivalents and the

resulting equation is divided by $\int_0^L \varphi_n^2(X) dX$, this yields:

$$\omega_n^2 q_n + 2\zeta_n \dot{q}_n + \ddot{q}_n = -\ddot{\Theta}_b \frac{\int_0^L X \varphi_n(X) dX}{\int_0^L \varphi_n^2(X) dX} + \frac{\varphi_n(L) F_{ye}}{\rho A \int_0^L \varphi_n^2(X) dX} \quad (B.1.10)$$

$$\omega_n^2 q_n + 2\zeta_n \dot{q}_n + \ddot{q}_n = -\alpha_n \ddot{\Theta}_b + \frac{\varphi_n(L) F_{ye}}{\mu_n} \quad (B.1.11)$$

where:

$$\alpha_n = \frac{\int_0^L X \varphi_n(X) dX}{\int_0^L \varphi_n^2(X) dX}; \quad \mu_n = \rho A \int_0^L \varphi_n^2(X) dX = \frac{\rho A L}{4} \quad (B.1.12)$$

some values of α_n are calculated in Appendix B.2

B.2 Calculation of α_n

In equation B.1.12 α_n is defined as:

$$\alpha_n = \frac{\int_0^L X \varphi_n(X) dX}{\int_0^L \varphi_n^2(X) dX} \quad (\text{B.2.1})$$

If we want to simulate the beams behaviour we need to calculate some values of α_n . This is done with a Matlab program called `alphan.m` which is listed in Appendix E. The results of the first six values are listed in table B.1.

Table B.3 some values of $\alpha_n(L)$ ($L=0.430$ m)

n	$\alpha_n(L)$
1	0.48919
2	0.07806
3	0.02788
4	0.01423
5	0.00861
6	0.00576

Appendix C

To obtain a suitable equation for state space notation equation 3.2.7 is transformed into:

$$\ddot{\underline{p}} = (I + F)^{-1}(-\underline{\alpha}\underline{\theta}_b - R\dot{\underline{p}} - W\underline{p}) \quad (C.1)$$

or:

$$\ddot{\underline{p}} = F^*(-\underline{\alpha}\underline{\theta}_b - R\dot{\underline{p}} - W\underline{p}) \quad (C.2)$$

where:

$$F^* = (I + F)^{-1}$$

and:

$$\ddot{\underline{p}} = \underline{q}$$

Where I is the identity matrix. In state space notation equation C.2 will be denoted as:

$$\dot{\underline{x}} = A\underline{x} + \underline{b}u \quad (C.3)$$

$$\underline{x}^T = [\underline{\theta}_b, p_1, \dot{p}_1, p_2, \dot{p}_2, \dots, p_n, \dot{p}_n] \quad (C.4)$$

To obtain a suitable equation for state space notation we substitute equation C.2 in equation 3.3.3. This yields:

$$\dot{\underline{\theta}}_b = -r\underline{\phi}^{II^T}F^*(\underline{\alpha}\underline{\theta}_b + R\dot{\underline{p}} + W\underline{p}) + K_A u \quad (C.5)$$

For matrix A this results in:

$$A = \begin{bmatrix} -r\underline{\phi}^{II^T}F^*\underline{\alpha} & -r\underline{\phi}^{II^T}F_{11}^*R_{11} & -r\underline{\phi}^{II^T}F_{11}^*W_{11} & \dots & -r\underline{\phi}^{II^T}F_{nn}^*R_{nn} & -r\underline{\phi}^{II^T}F_{nn}^*W_{nn} \\ -F_{11}^*\alpha_1 & -F_{11}^*R_{11} & -F_{11}^*W_{11} & 0 & \dots & 0 \\ 0 & 1 & 0 & 0 & \dots & 0 \\ -F_{22}^*\alpha_2 & 0 & 0 & -F_{22}^*R_{22} & \dots & 0 \\ \vdots & \vdots & \vdots & \vdots & \ddots & \vdots \\ -F_{nn}^*\alpha_n & 0 & 0 & \dots & -F_{nn}^*R_{nn} & -F_{nn}^*W_{nn} \end{bmatrix}$$

and:

$$\underline{b}^T = [K_A, 0, 0, \dots] \quad (C.6)$$

The output relation in state-space notation will be described by the following equation:

$$\underline{y} = C\underline{x} + du \quad (C.7)$$

where:

$$\underline{y}^T = [\Theta_b, q_1, q_2, \dots, q_n, \Theta_0] \quad (C.8)$$

$$C = \begin{bmatrix} 1 & 0 & 0 & 0 & \dots & 0 \\ -F_{11}^* \alpha_1 & -F_{11}^* R_{11} & -F_{11}^* W_{11} & 0 & \dots & 0 \\ \vdots & \vdots & \vdots & \vdots & \ddots & 0 \\ -F_{nn}^* \alpha_n & 0 & 0 & \dots & -F_{nn}^* R_{nn} & -F_{nn}^* W_{nn} \\ 1 - s_1 \underline{\alpha}^T & -s_1 R_{11} & -s_1 W_{11} & \dots & -s_n R_{nn} & -s_n W_{nn} \end{bmatrix} \quad (C.9)$$

$d=0$

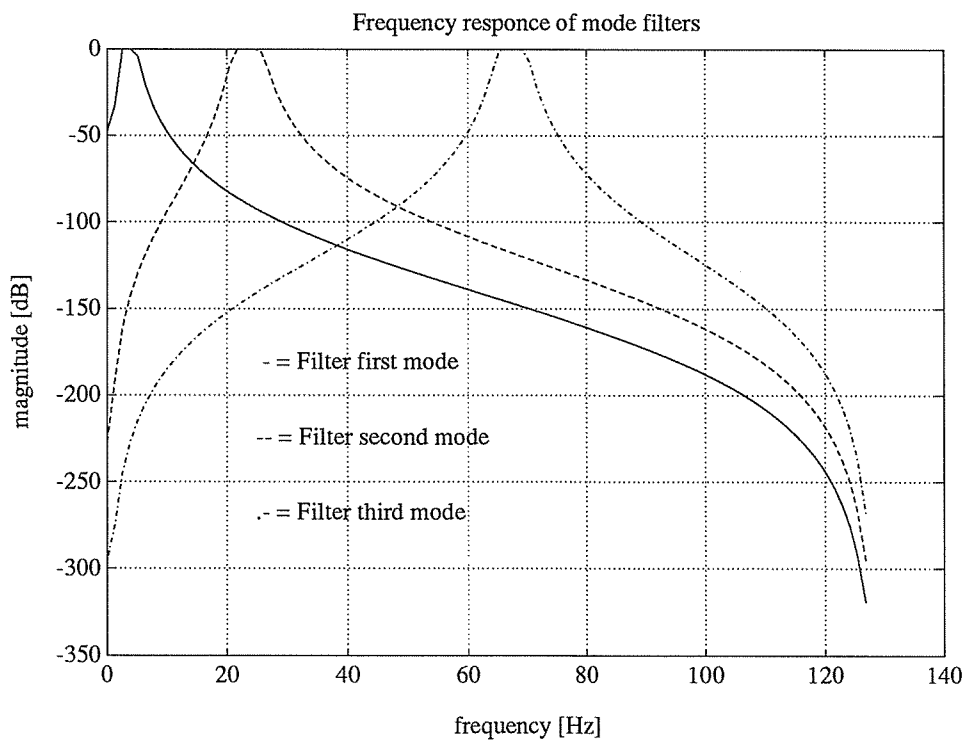
$$s_i = \frac{\varphi_i(L)}{L} F_{ii}^* \quad (C.10)$$

Appendix D

In section 4.2 stated that the values ζ_i could be derived by matching the filtered time-response with equation 4.2.4. The filters were designed with the Matlab routine Butter.m. This routine can design a bandpass filter of a specified order. Table D.1 specifies the frequency band of the used filters. Figure D.1 shows the frequency response of the filters. The filters were all of fifth order.

Table D.1 frequency bands Butterworth filter

mode number	frequency band (Hz)
1	2 - 5
2	21 - 26
3	65 - 70



After filtering the signal from figure 4.1 is divided into three components, representing the eigenmodes. Form figure D.2 shows that in this case the second mode is dominant. Also the start-up transients of the filters are clearly visible.

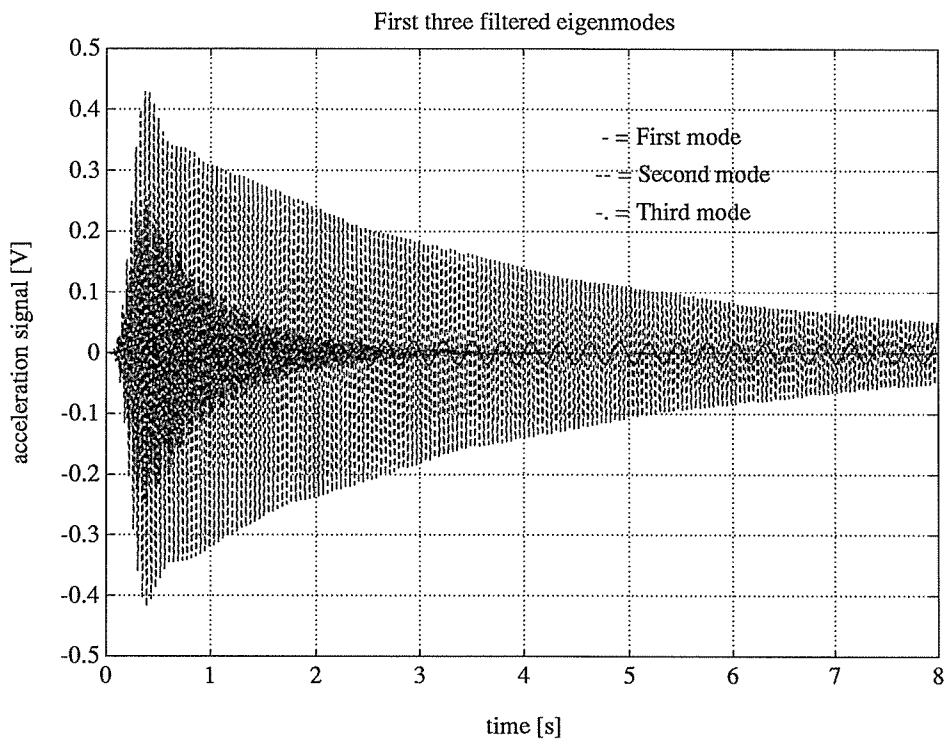


Figure D.2

We will now focus on the damping terms of the first two modes. Since the sample frequency is 256 Hz, the third mode won't be very accurate ($256 / 67.7 = 3.8$ samples per cycle). A Damped oscillation will be described by equation 4.2.4:

$$q_i(t) = A \cdot \sin(2\pi f_i t + \phi_i) \cdot e^{-\zeta_i \omega_i t} \quad (D.1)$$

Since the value of ϕ_i is of no importance to determine the damping of the oscillation, it will be set to zero. Figure D.3 and figure D.4 represent the fitting of the first and the second mode. The resulting damping terms follow from:

$$\zeta_1 \omega_1 = 0.042; \quad \zeta_1 = \frac{0.042}{\omega_1} = 0.0019 \quad (D.2)$$

$$\zeta_2 \omega_2 = 0.265; \quad \zeta_2 = \frac{0.265}{\omega_2} = 0.0018 \quad (D.3)$$

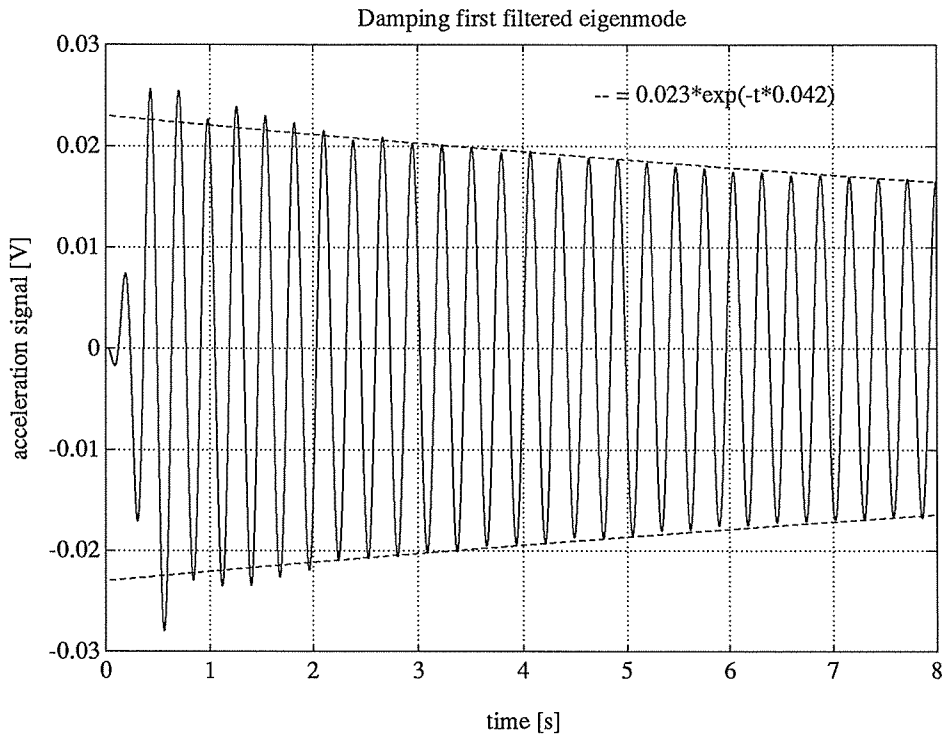


figure D.3

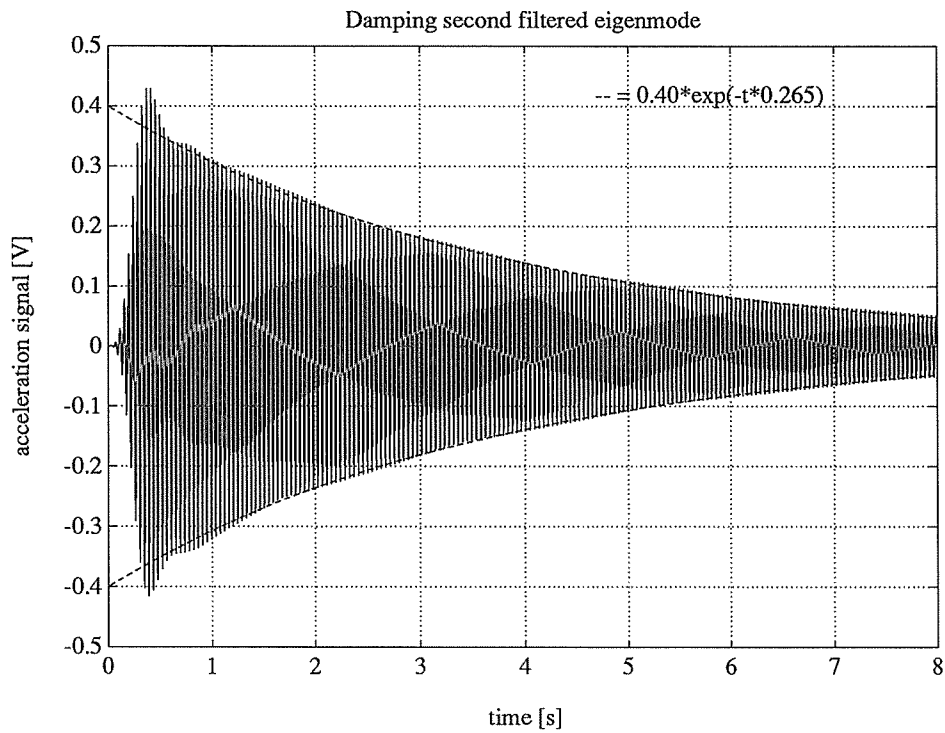


figure D.4

Appendix E

Program listings

SIMBEAM.M

This program defines or calculates all parameters or variables necessary to generate the state-space matrices that can be used to simulate the dynamic behaviour of a flexible beam.

```
%      simbeam.m simulates the movement of a flexible beam actuated
%      by a servo system who's input is a desired position of the beam tip.
%
```

```
%clearing
```

```
clear; clc; clg;
```

```
%declare globals
```

```
global L ii
```

```
one=1;
```

```
zero=0;
```

```
%define actuator parameters
```

```
%voltage- and torque constant
```

```
km(1)=0.19099; km(2)=0.195;
```

```
%armature resistance and armature inductance
```

```
Re=7.3; le=4.09e-3;
```

```
%armature inertia
```

```
Jm=3.727e-5;
```

```
 Km=km(1);
```

```
%define gearbox parameters
```

```
%transmission ratio and efficiency
```

```
ngear=10; %efficiency > 90
```

```
%maximum backlash: 3 arc min., torsional stiffness is 3.5 (Nm/min.)
```

```
%moment of inertia reflected to input shaft
```

```
Jg=8e-6;
```

```
%define powersystem parameters
```

```
%voltage- and current gain
Kpa=40; % Kpa(2);
%analog velocity feedbackgain (Vs)
Kd=1; Kdacc=Kpa*Kd/ngear;
%approximated transferfunction (constant gain) of motor
Ka=Kpa/(ngear*(Km+Kdacc));

%define desired movement

simt=4;
dt=0.01;
t=0:dt:simt;
%Desired Hub Angle
dha=pi/4
ttd=0;

%define mass payload
mp=0.010

%define flexible beam parameters

%length of the beam
%L=input('length of beam: ');
L=0.43; l=L;

%beam material: mat=1 => aluminum, mat=2 => steel
mat=1;

%cross-section (0.001*0.030), Young's modulus of elasticity, cross-
%sectional area moment of inertia and the mass density
Opp=3e-5; E=(7e10 2.2e11); I=2.5e-12; rho=(2.7e3 7.8e3);
parm=(Opp E(mat) I rho(mat));

%number of modes to simulate
ns=2

%number of modes to control
nc=2

%damping terms
ksi=(4.1e-3;2.9e-3;1.7e-3;5e-4;3.8e-4;2.6e-4;1.0e-4);

%calculate coefficients frequency-equation
gmil=gammi(ns);
(ci1,ci2)=cis(ns,gmil);
```

```

%calculate square angular resonace frequencies
(W,F)=calcw(mp,ns,gmiL,parm);
Fst=inv(eye(ns)+F);
Wmp=diag(sort(eig(Fst*W)));

%calculate G, phidxdxnul,phiL, alphan, r
%compose damping matrix
G=zeros(nc,ns);
for ii=1:ns,
    if ii <= nc,
        G(ii,ii)=one;
    end
    phidx2nul(ii)=phidx2(zero,gmiL,ci1,ci2);
    phiL(ii)=phi(1,gmiL,ci1,ci2);
    alfpan(ii)=alphan(mp,parm,phiL);
    for j=1:ns,
        if ii == j,
            R(ii,j)=2*ksi(ii)*sqrt(W(ii,j));
        else
            R(ii,j)=zero;
        end
    end
end
end
r=parm(2)*parm(3)*Re/((Km+Kdacc)*Km*ngear^2);

%compose state space system
(A,b,C,d)=state(ns,W,R,Fst,G,phidx2nul,phiL,alfpan,r,Ka);

%design optimal controler
(Ac,bc,Cc,dc)=state(nc,W,R,Fst,G,phidx2nul,phiL,alfpan,r,Ka);
Q=0.1*eye(2*nc+1); Rlqg=0.1;
(K,S)=lqr(Ac,bc,Q,Rlqg);

disp('Do you want to run a simulation now ?')
disp('variables XX YY and U will be overwritten !')
answer=input('Yes or No ? ','s');
if strcmp(answer,'y');
    (YY XX U K KK KKK)=simulat(A,b,C,d,t,dt,dha);
end

```

STATE.M

```
function (A,b,C,d)=state(n,W,R,Fst,G,phidx2nul,phiL,alfpan,r,Ka)
```

```
%(A,b,C,d)=state(n,W,R,Fst,G,phidx2nul,phiL,alfpan,r,Ka)
```

```

%
% state.m composes the statespace matrices for an actuated flexible beam
% system. the system is defined as:
%
%          .
%          x = Ax + bu
%          y = Cx + du
%
%          .       .       .       ..
% x=(hubangle p1 p1 p2 p2 .. pn pn); p = q
%          .. .. ..
% y=(thetab q1 q2 .. qn theta0); thetab=hub angle; theta0=tip angle
% u=(input voltage/-current of the actuatorsystem)

```

```
global L
```

```

gm1=-r*phidx2nul*Fst*alfpan';
C=zeros(n+2,2*n+1); C(1,1)=1; C(n+2,1)=1-(phiL/L)*Fst(1,1)*alfpan';
for i=1:n,
    gm2(1,2*i-1)=-R(i,i)*Fst(i,i)*r*phidx2nul(i);
    gm2(1,2*i)=-W(i,i)*Fst(i,i)*r*phidx2nul(i);
    bm(2*i-1,1)=-alfpan(i)*Fst(i,i);
    bm(2*i,1)=0;
    Am(2*i-1,2*i-1)=-Fst(i,i)*R(i,i);
    Am(2*i-1,2*i)=-Fst(i,i)*W(i,i);
    Am(2*i,2*i-1)=1;
    Am(2*i,2*i)=0;
    C(i+1,1)=-Fst(i,i)*alfpan(i);
    C(i+1,2*i)=-Fst(i,i)*R(i,i);
    C(i+1,2*i+1)=-Fst(i,i)*W(i,i);
    C(n+2,2*i)=-R(i,i)*Fst(i,i)*phiL(i)/L;
    C(n+2,2*i+1)=-W(i,i)*Fst(i,i)*phiL(i)/L;
end
A=(gm1 gm2
    bm Am);

b=zeros(2*n+1,1);
b(1)=Ka;
d=zeros(n+2,1);

```

GAMMI.M

```

function gmIL=gammi(n)

%gmIL=gammi(n)
%
% gammi.m calculates the first 'n' solutions to the

```

```
% frequency-equation 'cosh(gmiL)*cos(gmil)+1=0' with the initial
% values: (1.875, 4.69, 4.69+i*pi). The accuracy of the calculation
% equals 'epsil'. 'epsil'= 1e-16
```

```
epsil=1e-16;
gmm=(1.875);
for i=2:n,
    gmm(i)=4.69+(i-2)*pi;
end
for i=1:n,
    gmiL(i)=fzero('freqeq',gmm(i),epsil);
end
```

CI.M

```
function (ci1,ci2)=ci(n,gmiL)

%(ci1,ci2)=ci(n,gmiL)
%
% ci.m calculates the values of ci1 en ci2 for the calculation of phi(x) of the
% first n modes. gmiL contains the coefficients resulting from the frequency-
% equation and is generated with gammi.m.

for i=1:n,
    gl=gmiL(i);
    ci2(i)=-(cos(gl)+cosh(gl))/(2*(sin(gl)+sinh(gl)));
end;
ci1=0.500*ones(1,n);
```

SIMULAT.M

```
function (YY,XX,U,K,KK,KKK)=simulat(A,b,C,d,t,dt,dha,nc)

%(YY,XX,U,K,KK,KKK)=simulat(A,b,C,d,t,dt,dha)
%
% simulat.m simulates an actuated flexible beam system defined in simbeam.m.
% 'A b C d' represent the systems state space matrices. 't' is the time-axis to
% simulate and 'dt' is the timestep of the simulation. 'dha' is the Desired Hub-
% Angle (setpoint).

K=input('angle feedback gain: ');
KK=input('first mode feedback gain: ');
KKK=input('second mode feedbackgain: ');
```



```
%simulation
n=length(A);
T=(); YY=(); XX=(); U=(); X=zeros(2,n); u=(0; 0);
tk=zeros(n,1); tk(1)=-K; tk(2)=-KK; tk(3)=KKK;
%for i=1:nc,
%    tk(2*i)=-Kd*(10^(2+i));
%end
for i=1:length(t);
    u=(u(2) K*spd+Y(2,:)*tk);
    (Y,X)=lsim(A,b,C,d,u,(t(i); t(i)+dt),X(2,:));
    YY=(YY; Y(1,:)); XX=(XX; X(1,:)); U=(U u(2));
end
```

Appendix F

Technical data

Accelerometer:

- Type: Bruel & Kjaer 1704
- Mass: 2.11 g

Potentiometer:

- Type: MCB PP 27
- Resistance: 2.2 k Ω
- Independent linearity: $\pm 1\%$
- Starting and running torque: ≤ 0.014 Nm
- Moment of inertia: $\leq 10^{-7}$ kgm²
- Maximum rotation speed: 120 rpm = 12.57 rad/s

Servomotor:

- Type: GSC 5DA08 (DC Servomotor)
- Rated power: 80 W
- Rated Torque: 0.260 Nm
- Voltage constant: $20.0 * 10^{-3}$ V/rpm = $3.33 * 10^{-4}$ Vs / rad
- Mechanical time constant: 5.5 ms; $f_{max} = 182$ Hz
- Electrical time constant: 0.57 ms; $f_{max} = 1754$ Hz
- Armature inertia: $2.746 * 10^{-5}$ kgm²

Gearbox:

- Type: Micron planetary gearhead 'size 6' (single stage)
- Reduction ratio (i): 10 (-)
- Maximum backlash: 3 arc min.
- Rated output torque (mean): 23 Nm (at 1000 rpm)
- Mass moment of inertia: $8.0 * 10^{-6}$ kgm² (reflected to input shaft)

Digital Signal Processor:

- Type: Loughborough Sound Images Ltd. 69002
- Peak performance: 50 Mflops
- Continuous performance: 33 Mflops